Energy & Environmental Science

Accepted Manuscript

This article can be cited before page numbers have been issued, to do this please use: Q. Wang, N. Phung, D. Di Girolamo, P. Vivo and A. Abate, *Energy Environ. Sci.*, 2019, DOI: 10.1039/C8EE02852D.

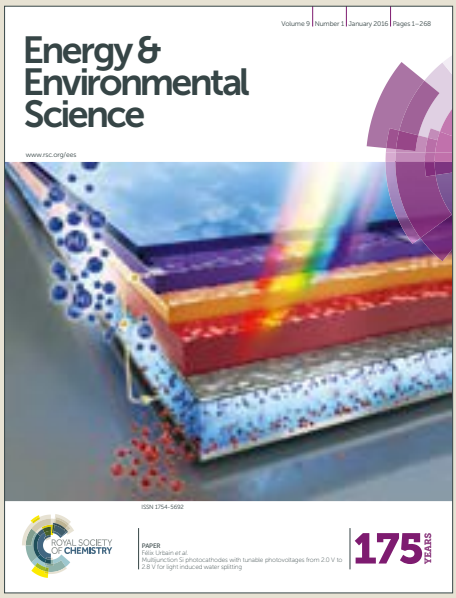

ROYAL SOCIETY OF CHEMISTRY

rsc.li/ees

View Article Online
DOI: 10.1039/C8EE02852D

Enhancement in Lifespan of Halide Perovskite Solar Cells

Qiong Wang[1], Nga Phung[1], Diego Di Girolamo[2], Paola Vivo[3], and Antonio Abate[1,4,5]*

[1] Helmholtz-Zentrum Berlin für Materialien und Energie, Kekuléstraße 5, 12489 Berlin, Germany

[2] Department of Chemistry, Sapienza University of Rome, 00815 Rome, Italy

[3] Laboratory of Chemistry and Bioengineering, Tampere University of Technology, P.O. Box 541, FI-33101 Tampere, Finland

[4] Institute of Advanced Energy Materials, Fuzhou University, Fuzhou, Fujian 350002, China.

[5] Department of Chemical, Materials and Production Engineering, University of Naples Federico II, Piazzale Tecchio 80, 80125 Fuorigrotta, Naples, Italy

*Corresponding author: A.A. antonio.abate@helmholtz-berlin.de

antonio.abate@unina.it

View Article Online
DOI: 10.1039/C8EE02852D

Abstract

While perovskite solar cells have skyrocketed in recent years to power conversion efficiencies competitive with those of silicon and thin-film photovoltaics, the lagged behind stability stands in the way of commercialisation. In this review, we discuss the reasons and factors that induce the degradation in photovoltaic performance of perovskite solar cells, and furthermore, we summarise the most promising strategies to enhance the lifespan. We show that each component of the device, including charge selective contacts, perovskite layer, and electrodes, can be engineered to reduce the influence of heat, UV light, oxygen, moisture and their synergetic effect on the operating lifetime of devices. We conclude that inorganic contacts and inorganic perovskite compositions are the most promising direction toward stable perovskite solar cells.

Keywords

Perovskite solar cells; Degradation; Lifespan; Stability; Ageing protocol; All inorganic perovskite photovoltaics

View Article Online
DOI: 10.1039/C8EE02852D

Table of Contents

View Article Online
DOI: 10.1039/C8EE02852D

1. Introduction

Halide perovskite semiconductors exhibit outstanding optoelectronic properties,[1] such as high absorption coefficient,[2, 3] sharp band edge,[4, 5] tuneable optical band gaps spanning from visible to near-infrared wavelength range,[6, 7] high defect tolerance,[8] and low exciton binding energy[9]. The application of halide perovskites goes from photovoltaics[10], light emitting diode[11], photo-detectors[12], memory devices[13] to solar batteries[14]. Furthermore, halide perovskites can be processed by almost all standard thin film deposition techniques, including thermal evaporation,[15] spin-coating,[16-18] dip-casting,[19] atomic layer deposition (ALD),[20] screen printing,[21, 22] inject printing,[23] and roll-to-roll printing.[21, 24, 25] The outstanding optoelectronic properties in combination with the flexible processing make halide perovskites one of the most attractive materials for the electronic industry of the future.

The pioneering work was conducted by Miyasaka *et al.* in 2009 who applied methylammonium lead iodide ($MAPbI_3$) and methylammonium lead bromide ($MAPbBr_3$) as sensitisers in dye-sensitised solar cells.[26] The breakthrough in the power conversion efficiency (PCE) of perovskite solid-state solar cells was made in 2012, going beyond 10%.[27, 28] The value of PCE for perovskite solar cells (PSCs) quickly increased to over 20%,[29] with the current world record of 23.3% certified by NREL (National Renewable Energy Laboratory in the USA).[30] The low cost, highly efficient, and scalable PSCs are the most promising candidates to enter the photovoltaic market that is currently dominated by silicon and thin-film solar cells. Although the overall efficiency of PSCs has increased over the years, the poor device stability is a major impediment to the commercialisation of PSCs.[31] **Figure 1** summarises the growth in efficiency of PSCs as well as the lifetime evaluated from T_{S80},[32, 33] *i.e.* the corrected T_{80} for PSCs taking into consideration the reversible loss during the day/night cycling - the time that takes for the PCE drops to 80% of its initial value, - and energy generation during the lifespan of PSCs based on the analysis of the literature data published from the year of 2013 to 2018. It clearly shows that the lifetime of PSCs is limited to 3,000 hours, which is far away from the standard solar cells, *i.e.* up to 25 years of operational lifetime. In other words, it is urgent to enhance the lifespan of PSCs to meet the high expectations for a newly emerging PV.

We will review the measurement methods for the assessment of the operational stability of PSCs. Then we will discuss the most promising material, device, and interface engineering approaches to extend the operational lifetime of PSCs.

View Article Online
DOI: 10.1039/C8EE02852D

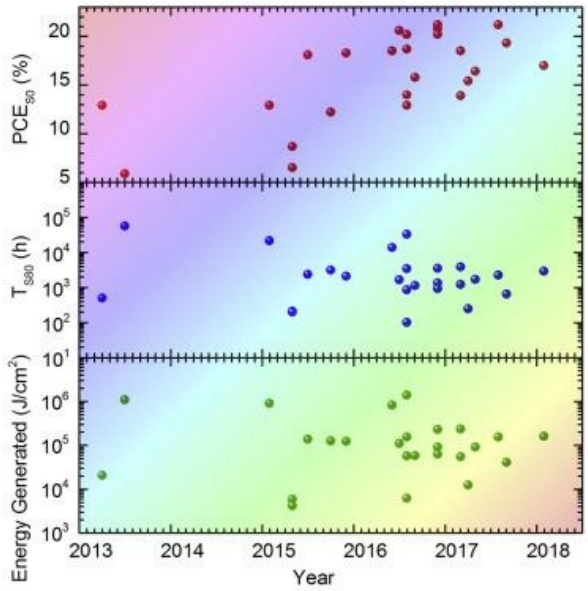

Figure 1. Summary of literature data published from the year of 2013 to 2018 related to PCE_{80} (top panel), T_{S80} (middle panel), and generated energy of PSCs (bottom panel).[32] Reproduced with permission from ref.[32]. Copyright 2018, Elsevier.

2. Lifetime evaluation

Most of the studies on the stability of PSCs reported the performance measured periodically for a prolonged time using a single current-voltage measurement or *JV* scan. In between two consecutive *JV* scans, the devices were either stored in the dark or kept under continuous illumination at open circuit, the so-called "light soaking" test. For organic photovoltaics, the stability testing of devices stored in the dark and measured periodically is referred to as the shelf life testing - ISOS-D-1 protocol.[34] However, a testing protocol similar to the ISOS-D-1 would not provide a reliable estimation of the PSC stability. Indeed, the efficiency of PSCs as extracted from the *JV* scan can be different from the actual power output extracted from the maximum power point tracking (MPPT) after a prolonged light soaking or dark storage. The difference between the *JV* and the MPPT is mainly due to the presence of hysteresis, *i.e.* the difference in *JV* curves under forwarding (from low bias to high bias) and reverse (from high bias to low bias) scans in PSCs and device degradation under continuous illumination.[35] In particular, in our recent publication,[33] we demonstrated that the lifetime could be overestimated or underestimated depending on the device architecture.

Based on the above discussion, we believe that it is necessary that the research community adopts a standard protocol for stability testing of PSCs. We[33] proposed a testing protocol that includes MPPT measurement for at least 150 hours under illumination and testing after dark resting for several hours. The significance of this protocol is that it includes consideration for:

View Article Online
DOI: 10.1039/C8EE02852D

i) the hysteresis in PSCs that makes the *JV* scans rather ineffective to estimate the actual power output after prolonged ageing. *ii)* The "burn-in" time, *i.e.* non-recoverable permanent degradation occurring at the beginning of the device operation. It is important to note that the "burn-in" time is considered in the ageing protocols of organic solar cells and silicon solar cells as well. *iii)* The "reversible losses or gain", *i.e*. the efficiency gains or losses that can be obtained by re-measuring the device after resting in the dark. The "reversible losses" in PSCs are widely observed in regular structured PSCs (n-i-p architectures). *iv)* A figure of merit for stability, such as the T_{S80} that provides the time at which the device has degraded to 80% of its initial efficiency. After that, the device should be replaced as more serious degradation mechanisms may start kicking in. The T_{80} value is well-established for silicon solar cells and thin-film solar cells. This parameter provides accessible information for comparison between different technologies.

Also, Tiihonen *et al*.[36] pointed out the worrying practice that most of the works in the literature reported data from a single device to conclude about stability – lack of statistical analysis. Nevertheless, we are also aware that testing the stability for a statistically significant number of PSCs may be rather impractical on a lab scale. Therefore, we recommend careful consideration before providing the conclusive data from a non-statistical number of devices.

3. Each component in PSCs matters

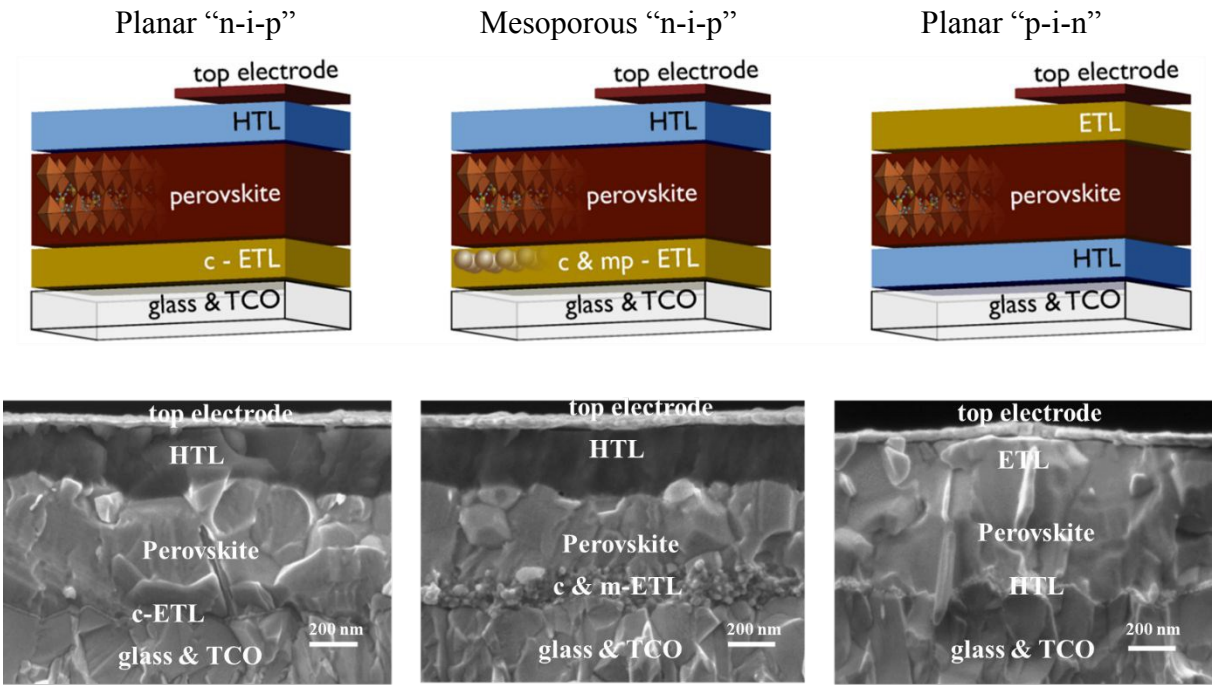

Figure 2. Schematics (top panel) and cross-sectional SEM images (bottom panel) of planar regular PSCs, regular mesoporous PSCs, and planar inverted PSCs with a scale bar of 200 nm.[37] Reproduced with permission from ref.[37]. Copyright 2018, American Chemistry Society.

A highly efficient PSC is generally composed of an effective electron and hole selective contact, and a compact and dense perovskite film. PSCs can be classified into regular ("n-i-p") and inverted ("p-i-n") architectures based on the sequence of the layers comprising the device. Regular architectures are made by transparent conductive glass (TCO)/electron selective contact (ESC)/perovskite film/hole selective contact (HSC)/metal contact, while inverted structures employ TCO/HSC/perovskite/ESC/metal contact. Under illumination, photo-generated electrons are injected from the perovskite film to the bottom ESC in regular PSCs ("n-i-p") or the top ESC in inverted PSCs ("p-i-n"). Regular PSCs can be further classified into "mesoporous", containing a mesoporous ESC, and "planar", containing a compact ESC. The schematics and cross-sectional scanning electron microscopy (SEM) images of regular and inverted PSCs are given in **Figure 2**.[38]

3.1 Electron selective materials (ESMs)

An efficient electron selective material (ESM) should meet several criteria, such as high electron mobility, low concentration of deep trap states, good energy alignment with other components in the device, and ideally inexpensive in production. ESMs can be inorganic semiconductors or organic molecules.

3.1.1 Inorganic electron selective materials

Inorganic electron selective materials (ESMs), such as metal oxides, are intrinsically more stable than organic ESMs under the influence of temperature, humidity, oxygen, and UV light. Inorganic ESMs, which normally need high-temperature annealing and processing with polar solvents, are broadly used in "n-i-p" PSCs that allow the deposition of ESMs ahead of the perovskite film. One of the most commonly used inorganic ESMs is titanium dioxide (TiO_2).[39] In the most efficient configuration, the TiO_2 contact is constituted by stacking compact (c-TiO_2) and mesoporous (m-TiO_2) films.[40] There are several ways to deposit the c-TiO_2 film, such as spin-coating, spray pyrolysis, or atomic layer deposition (ALD). TiO_2 mesoporous film (m-TiO_2) is normally deposited from a TiO_2 paste, where TiO_2 nanoparticles are mixed with solvents, such as ethanol and terpineol and organic linkers, such as ethyl cellulose pre-dissolved in ethanol. In most cases, both c-TiO_2 and m-TiO_2 need to be annealed at 450 °C to get an anatase phase TiO_2. The low-temperature deposited TiO_2 planar film has also been reported in a few cases.[41, 42] However, due to the low conductivity in intrinsic TiO_2, planar PSCs employing

View Article Online
DOI: 10.1039/C8EE02852D

TiO_2 ESM present a huge hysteresis. On the contrary, the mesoporous structured PSCs that employ TiO_2 mesoporous film enlarge the interface area between TiO_2 nanoparticles and perovskite film, showing significant suppression of the hysteresis.[43] Chemical doping, such as lithium ions (Li^+) can enhance the electron conductivity of TiO_2,[44] which promoted the efficiency of PSCs from 17% for the pristine TiO_2 to over 19% for the Li^+ doped TiO_2 mesoporous film. Till now one of the highest reported efficiencies of 22.1% was achieved by the regular PSCs containing m-TiO_2.[40]

However, Leijtens *et al.*[45] found that TiO_2 could bring some negative effects to the stability of PSCs under the illumination of UV light. TiO_2, with an energy band gap of around 3.2 eV, shows a strong absorbance in the short-wavelength range and is a UV photocatalyst. This led to the oxidation of the absorbed oxygen into oxygen radicals that were highly oxidative, hence resulting in the decomposition of the adjacent perovskite layer.[46] One recent study introduced a plant sunscreen material, *i.e.* sinapoyl malate, between the TiO_2 layer and the perovskite film as a scavenger for the oxygen radicals, resulting in a significant enhancement of the PSCs stability under UV light exposure.[47]

In the last two years, another inorganic ESM, *i.e.* tin oxide (SnO_2 or SnO_x), was introduced into the PSC system. SnO_2 has been applied as an ESM in dye-sensitised solar cells (DSCs) before and has demonstrated its excellent electronic property in a DSC system.[48] In 2015, Correa-Baena *et al.*[49] introduced the ALD-prepared SnO_2 planar layer in PSCs, and they observed a substantial suppression in the hysteresis compared to TiO_2 contained PSCs. Later, Roose *et al.*[50] introduced Ga-doped SnO_2 mesoporous layer (m-SnO_2) into PSCs. They measured the stability of PSCs with a periodic "light-soaking" under full spectrum illumination (AM 1.5 G, 100 $mWcm^{-2}$) inside the N_2 filled glove box. They found that both m-SnO_2 and m-TiO_2 based PSCs had a "burn-in" time, showing a rapid drop to 80% within the first 100 hours of "light soaking". After "burn-in" time, m-SnO_2 based PSCs stabilised at around 70% of the initial PCE for up to 1000 hours. In contrast, m-TiO_2 based PSCs left only 20% of the initial value. After ~ 1000 hours of illumination, they stored PSCs in the dark for 200 hours, and then tested the *JV* curves of these devices again. Differently from the reported "self-healing" of PSCs after dark storage,[51] they did not observe any notable recovery in the efficiency, which brings questions to the long-term photo-stability (up to 1000 hours continuous illumination) of perovskite compounds and HSCs during the "light soaking" process.

View Article Online
DOI: 10.1039/C8EE02852D

3.1.2. Organic electron selective materials

As mentioned above, organic compounds are not as stable as inorganic metal oxides. In most cases, organic compounds need to be stored inside an N_2-filled glove box in the dark. Decomposition of organic materials can be triggered by UV light radiation, oxidation in air, and moisture absorption. Because organic ESMs can be processed at low temperatures and dissolved in solvents, such as chlorobenzene that has negligible influence on the perovskite films, they are mainly used in inverted ("p-i-n") structured PSCs, where the ESMs are deposited on top of perovskite.

Fullerene and its derivatives have been the most commonly used organic ESMs because of their well-known excellent electronic conductivity. They are efficient ESMs in organic photovoltaics and are commercially available. Phenyl-C_{61}-butyric acid methyl ester (PCBM) and C_{60} are the most popularly used derivatives of fullerene. PCBM can be deposited from the solution *via* spin-coating, and C_{60} can be deposited *via* thermal evaporation. Both of them have a relatively high hydrophobicity. Some works replaced fullerene-based ESMs with polymeric ESMs[52], or fluorine functionalized graphene[53] that had a stronger hydrophobic property and resulted in enhanced moisture stability for devices stored in the dark at a controlled humid environment and in the "light-soaking" measurement. The most efficient inverted PSCs reported so far is based on C_{60} ESM, with a record of 21.4%.[54]

3.2 Perovskites

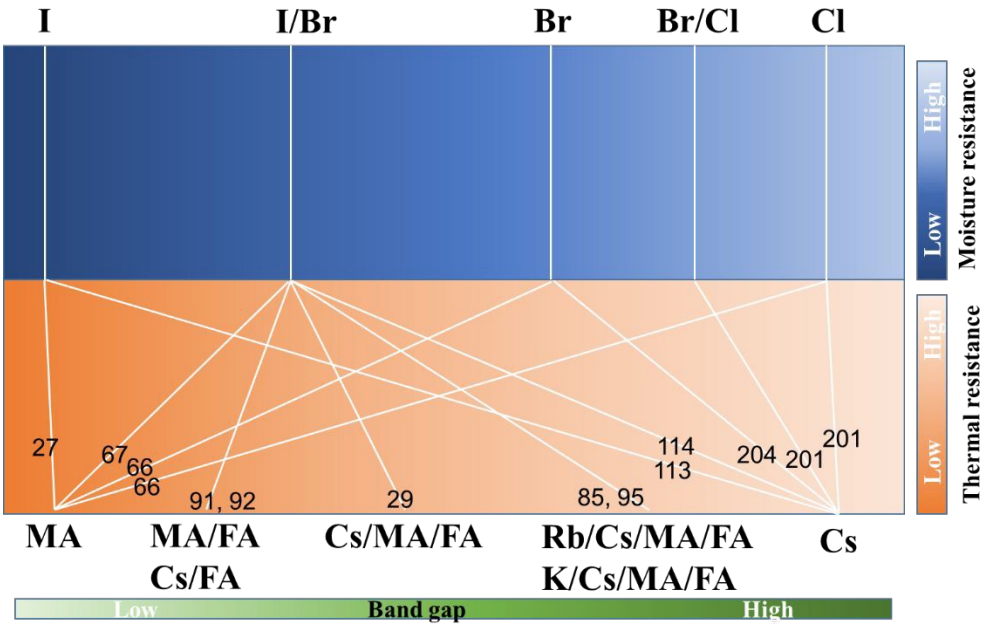

Scheme 1. Illustration of the intrinsic stability and bandgap of ABX_3 against moisture and heat influenced by cations and halides. The trends are extrapolated from literature discussed in the

View Article Online
DOI: 10.1039/C8EE02852D

main text. Selected references as the representative of each perovskite compositions are labelled on the guidelines.

Halide perovskite is the key component in PSCs with a common formula of ABX_3, where A is a monovalent cation placed in the octahedral cage consisting of shared corners BX_6, being B a divalent metal and X a halide. Methylammonium lead iodide ($MAPbI_3$) based PSCs have achieved extraordinary high efficiency reaching more than 20%[55, 56] in recent years. However, they suffer from the degradation caused by external factors such as moisture,[57] heat,[58] oxygen,[59] and light.[60] Moreover, the synergetic effect of oxygen, heat and photo-illumination fastens the process of moisture-induced degradation.[61] Using a mixture of halides instead of pure iodide results in more robust moisture stability in the compound.[13, 62] This is partial because when perovskite is exposed to moisture, the formation energy of H-I bond is much smaller than that of H-Br and H-Cl, which breaks down the bonding of Pb-I in the crystal structure of perovskite.[63] Moreover, the poor thermal stability of $MAPbI_3$ is mostly attributed to the organic cation, *i.e.* MA^+.[64, 65] Alloying A-site cations, particularly inorganic cations, *i.e.* Cs^+ (caesium) and Rb^+ (rubidium), are found to significantly enhance the thermal stability of perovskite compounds.[29, 66] The influence of cation and halides on the intrinsic thermal and moisture stability of perovskites are illustrated in **Scheme 1**. In this Section, we will discuss the large family of perovskites of mixed halides and cations, mainly focusing on their vulnerability to photo-induced phase segregation, thermal and moisture-induced composition degradation, and present a critical review on the mechanisms that cause degradation in perovskite and efforts made towards the enhancement of the intrinsic stability of perovskite materials.

3.2.1 Halide-mixed perovskite

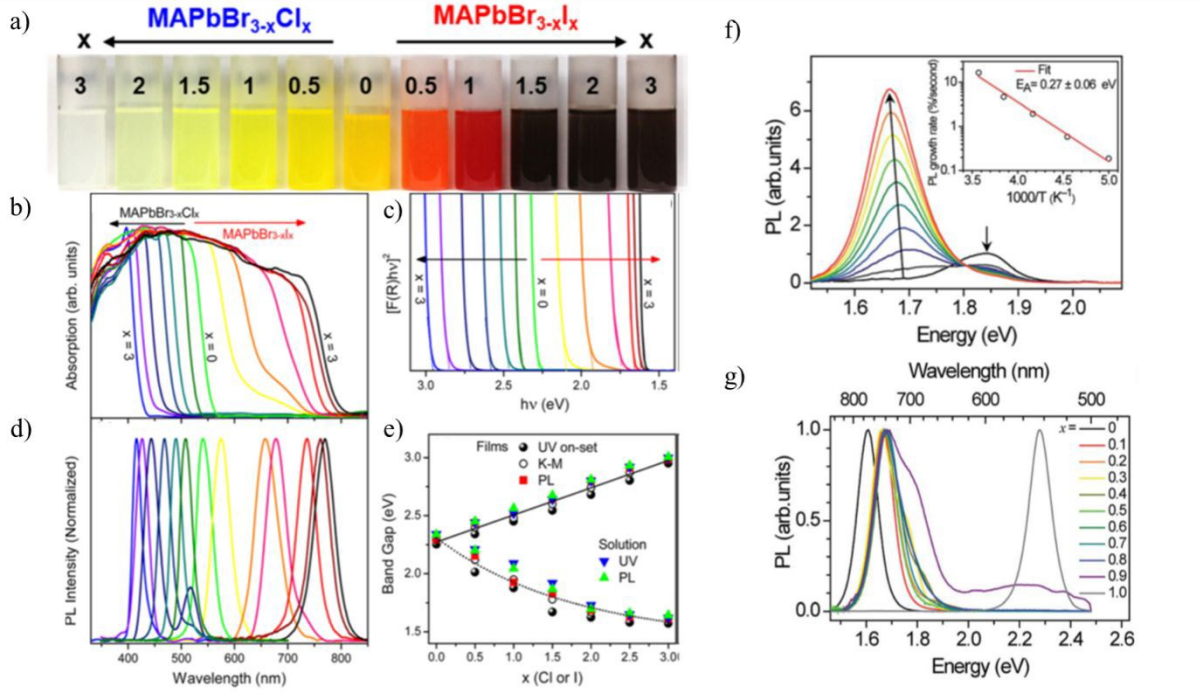

Figure 3. a) Digital photos; b) absorption spectra; c) absorption coefficients; d) steady-state photoluminescence (PL) spectra of perovskite films with mixed I/Br/Cl halides; e) dependence of the bandgap extracted from b)-d) on the ratio of halides (I/Cl) of mixed halide perovskites.[67] Reproduced with permission from ref.[67]. Copyright 2015, American Society of Chemistry. f) PL spectra of $MAPb(I_{0.6}Br_{0.4})_3$ perovskite films over 45 s in 5 s increments under 457 nm, 15 $mWcm^{-2}$ light at 300 K; g) normalised PL spectra of $MAPb(I_{1-x}Br_x)_3$ films with x ranging from 0 to 1 after illuminating for 5~10 minutes with 457 nm light at the intensity of 10-100 mW cm^{-2}.[68] Reproduced with permission from ref.[68]. Copyright 2015, Royal Society of Chemistry.

As we discussed at the beginning of this Section, perovskite of mixed halides exhibits better moisture stability than iodide only perovskites. Also, the optical bandgap of perovskites can be easily tuned by adjusting the halide ratio (*i.e.* I^-, Br^-, Cl^-) (**Figure 3)**. This is because the conduction and valence band positions of perovskites are largely determined by the hybrid orbitals of lead and halide. Thus, the changes in radii and the electron properties of halides from I^- to Cl^- can bring significant changes in the bandgap of the compounds.[69] **Figure 3a-e** shows the systematic studies of the dependency of the bandgap of $MAPbX_3$ (where X is I/Br/Cl) on halide ratios, ranging from 1.54 eV ($MAPbI_3$) to 2.44 eV ($MAPbCl_3$).[67] More importantly, in the broad range of bandgaps, all the mixed halide perovskites present a sharp absorption onset with a strong emission peak, which indicates the direct semiconductor nature of perovskites at room temperature with a high absorption coefficient. The superior optoelectronic properties of mixed halide perovskite were recently identified to be determined by the iodine chemistry in perovskite compounds. It was found that in the prototype of $MAPbI_3$, the less abundant iodine

View Article Online
DOI: 10.1039/C8EE02852D

defects and MA defects were identified as the source of photochemically active deep electron and hole traps in $MAPbI_3$.[70-72] Bromine and chlorine doping of $MAPbI_3$ helped to inactive hole traps. Mixed halide perovskites have been demonstrated successfully in photovoltaic applications as well as other optoelectronic devices, such as light emitting diodes (LEDs).[73]

Although mixed halide perovskites present superior stability to iodide only perovskites, the mixed halides composition brings a risk of halide segregation under continuous light illumination.[68] **Figure 3f** shows the steady-state photoluminescence (PL) spectra of $MAPb(I_{0.6}Br_{0.4})_3$ perovskite over 45 s in 5 s increments under 457 nm, 15 $mWcm^{-2}$ light at 300 K.[68] The decrease in the intensity of the emission peak assigned to mixed halide perovskite and the appearance of the emission peak assigned to $MAPbBr_3$ perovskite are clearly observed. Phase segregation induced by halide segregation generates new defects in the bulk of perovskite films and leads to fast degradation in photovoltaic performance of PSCs. Although the phase segregation can be recovered after storing in the dark for some minutes, it largely reduces the output power of PSCs, mostly due to the lost in V_{oc}. Fortunately, as shown in **Figure 3g**, Br content of less than 20% in $MAPb(I_xBr_{1-x})_3$ does not show phase segregation after illuminating for 5~10 minutes with 457 nm light at the intensity of 10-100 mW cm^{-2}, whereas Br content of over 20% show the second emission peak located in the shorter wavelength range of higher band gap.[68] As discussed in the following sections, the mixed halide ratio will be adjusted in conjunction with the mixed cations to stabilize the perovskite phase and to reach the ideal band gap in perovskite compounds.[68]

Meanwhile, the origin of halide segregation in the mixed halide perovskites is still under debate. It was suggested by Brivio *et al.*[74] that halide segregation was induced by photo-illumination, while Bischak *et al.*[75] found that the interaction between the photo-generated charge carriers and the polarons induced lattice strains that might promote halide segregation in the film. They observed that compared to the organic cations, such as MA^+; the less polarised Cs^+ in A-site showed a better photo-stability in mixed halide $CsPbX_3$ material.[75] Even the mixed cation of Cs/MA in Br-rich perovskite, *i.e.* $Cs_{0.39}MA_{0.61}Pb(I_{0.15}Br_{0.85})_3$ was reported not to experience any phase segregation.[76] Another work reported that a significant bulk strain was found in the mixed halide $MAPb(I_xBr_{1-x})_3$,[77] which led to the thermodynamically preferred segregation states.[77, 78] This observation was then supported by the pronounced mismatch in lattice between cubic $MAPbBr_3$ and tetragonal $MAPbI_3$.[79] It was also found that perovskite films with irregularity in the microstructure, *i.e.* non-compact and non-dense films were more likely to experience the halide segregation, especially those with a large abundance of grain boundaries.

Grain boundaries are preferable sites for halide segregation for two possible reasons: *i*) defects at the boundary can be an easy pathway for halide migration,[77, 80] and *ii*) lattice mismatch between iodide and bromide-rich material takes place only at grain boundary where the energy cost is lower than in bulk.[81] Advanced imaging techniques, such as PL mapping[82] and cathodoluminescence (CL) topology mapping overlaying with SEM image[75] showed more pronounced halide clusters near the grain boundaries. After that, it has been reported that the improvement of the crystal quality of the film suppresses this phenomenon.[81, 83] However, the halide segregation was also observed in single crystals by Hoke *et al.*[68] They concluded that the abundance of defects and grain boundaries were not prerequisite for halide segregation.[68] In contrast, several studies reported that defect reduction helped to enhance the photostability.[80, 83] Single crystals are also found to be more stable in regards to photo-induced phase segregation.[82] This could be related to the fact that ion migration occurred in single crystals required higher activation energy than in the polycrystalline films.[84]

3.2.2 Cation-mixed perovskite

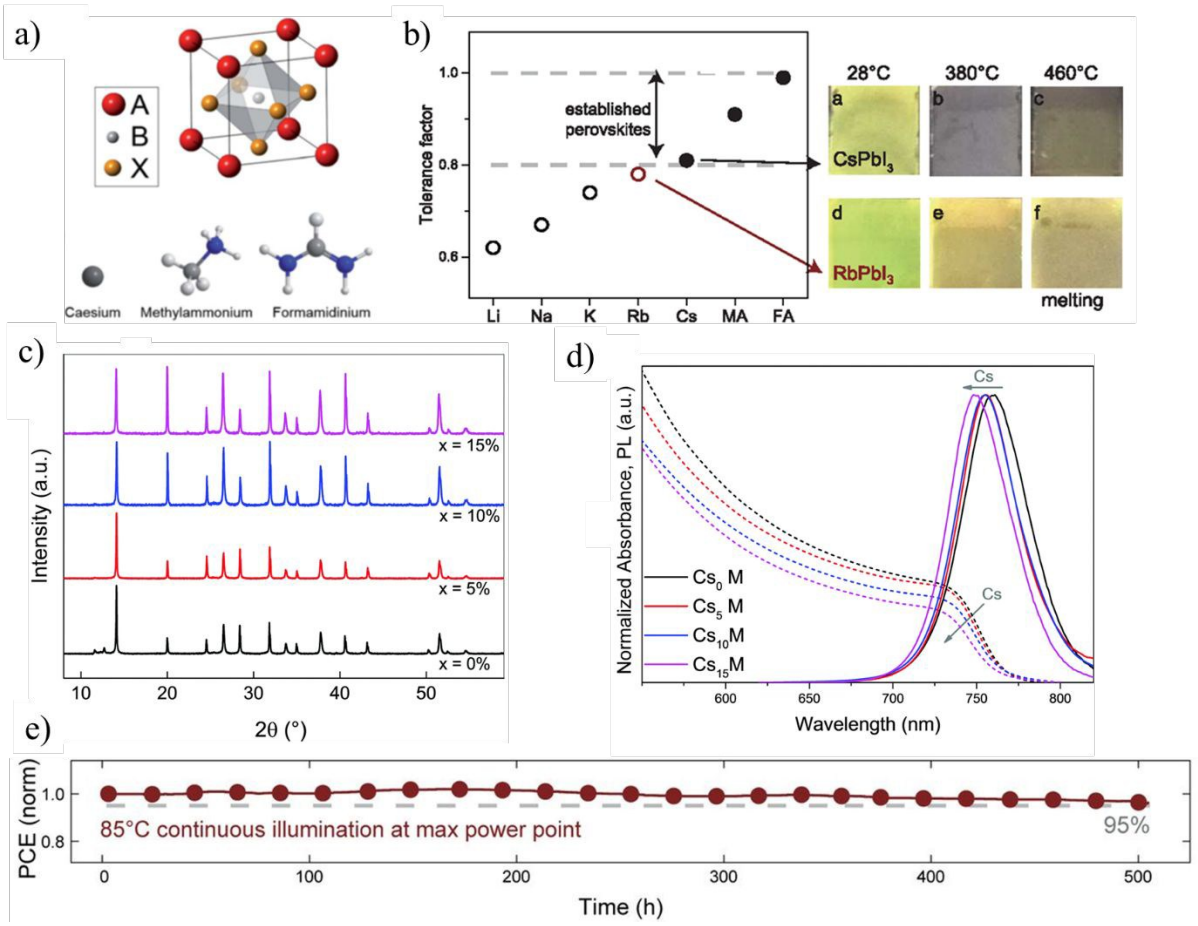

Figure 4. a) Scheme of the crystal structure of ABX_3 perovskite, where A site can be Cs^+, MA^+ or FA^+.[85] Reproduced with permission from ref.[85]. Copyright 2014, Royal Society of Chemistry. b) Tolerance factor plot for a range of monovalent cations at A site in $APbI_3$, with

the digital photos of $CsPbI_3$ and $RbPbI_3$ films at temperatures of 28 °C, 380 °C and 460 °C.[86] Reproduced with permission from ref.[86]. Copyright 2016, American Association for the Advancement of Science. Influence of Cs^+ in c) the crystal structure and d) optical bandgap extracted from absorption spectra and steady-state PL spectra of FAMA-double perovskite, *i.e.* $FA_{0.83}MA_{0.17}PbI_{0.83}Br_{0.17}$.[29] Reproduced with permission from ref.[29]. Copyright 2016, Royal Society of Science. e) MPP tracking of quadruple cation perovskite, RbCsFAMA devices measured at 85 °C in inert atmosphere.[86] Reproduced with permission from ref.[86]. Copyright 2016, American Association for the Advancement of Science.

Figure 4a shows the scheme of the crystal structure of ABX_3 with the molecular structure of the three most commonly used monovalent cations, *i.e.* Cs^+, methylammonium (MA^+), and formamidinium (FA^+). **Figure 4b** shows the Goldschmidt tolerance factor of a series of monovalent cations in A site of $APbI_3$ perovskite. Goldschmidt tolerance factor (denoted as *t*) depends on the effective radii of A, B, X in the crystal structure (**Figure 4a**), and is often used to assess the possible formation of three dimensional (3D) ABX_3 perovskite crystal. It can be expressed as equation 1 (Eq.1).

$$t = \frac{R_A + R_X}{\sqrt{2}(R_B + R_X)} \qquad \text{Eq.1}$$

Cations that show a tolerance factor in the range of 0.8 ~ 1 are expected to be able to form a 3D perovskite crystal. As shown in **Figure 4b**, Cs^+, MA^+, and FA^+ have the right radius for $APbI_3$ 3D perovskite, but Rb^+ is beyond the minimum limit of this parameter. Indeed, it was found that $CsPbI_3$ could be formed by annealing at a relatively high temperature at 300 °C.[87-89] In contrast, $RbPbI_3$ perovskite did not exist in practice; annealing at high temperatures melt the material (**Figure 4b**).[86]

i) Double cation perovskite

Although the organic cation has no direct contribution to the valence band and conduction band of the material, its shape and size affect the size of a unit cell and the bond angle of Pb-I that in turn influences the bandgap. Indeed, $FAPbI_3$ perovskite has a smaller bandgap of 1.48 eV[85] than that of $MAPbI_3$ (around 1.55 eV), and it is closer to the optimal bandgap set by the Shockley–Queisser limit for single junction solar cells.[90] Unfortunately, $FAPbI_3$ transforms into a yellow, non-photovoltaic phase (δ-phase) at room temperature from the active photovoltaic phase (α-phase) annealed at 160 °C.[91] The thermodynamic instability in α–phase $FAPbI_3$ perovskite is due to the large strain in the α-phase crystal structure that promotes the phase transition to the strain-free δ-phase structure. Experimentally, it has been found that introducing smaller cations, such as MA^+ or Cs^+ relaxed the strain and stabilised the α-phase.[66, 92] This was then supported

by theoretical calculations on Cs^+ doped $FAPbI_3$.[93] Due to the large difference in atomic arrangement and volume of the unit cells, it was difficult for δ-phase $CsPbI_3$ and $FAPbI_3$ to accommodate each other in one crystal structure, whereas their α-phases shared a similar value in sizes of unit cells and thus were thermodynamically suitable for mixing.[94] In particular, CsFA-double cation perovskite, *i.e.* $FA_{0.83}Cs_{0.17}PbI_{0.83}Br_{0.17}$ exhibits a suitable bandgap of ~ 1.74 eV and robust thermal stability and photo-stability and has been a good choice for the "top cell" in a stack with silicon solar cells.[95]

ii) Triple cation perovskite

The stabilisation of α-phase $FAPbI_3$ by MA^+ and Cs^+ inspired the triple cation system. Saliba *et al.*[29] developed the triple cation perovskite CsFAMA-PSC ($Cs_{0.05}(FA_{0.83}MA_{0.17})_{0.95}Pb(I_{0.83}Br_{0.17})_3$). **Figure 4c-d** show the enhanced crystallinity and slightly increased optical band gap under the influence of Cs^+ in the triple cation perovskite. Moreover, compared to the double cation perovskite, the triple cation perovskite exhibited a largely enhanced thermal stability and moisture stability due to the presence of the inorganic cation. Furthermore, the triple cation perovskite deposited by the anti-solvent method showed high crystallinity and facile formation of monolithic grains. Adopting the triple cation perovskite system, Saliba *et al.*[29] achieved a stabilised PCE of over 21% with a better reproducibility compared to MAFA-devices. The deposition of MAFA-double cation perovskite is found to be sensitive to the fabrication conditions. A small vibration in the temperature of the glove box can bring a huge impact on the final quality of perovskite films. Integrating Cs^+ into the system pushes black phase perovskite formation into a new energy-favourable equilibrium. Moreover, CsFAMA-PSCs exhibited a significant enhancement in device stability, holding 90% of its initial efficiency after 250 hours of constant illumination in MPPT measurement, while MAFA-PSCs degraded to less than 50% of its initial value after 100 hours of constant illumination in the MPPT measurement conducted at room temperature and in N_2 atmosphere.[29]

iii) Quadruple cation perovskite

As shown in **Figure 4b**, only Cs^+, MA^+ and FA^+ can form the 3D perovskite structure of $APbI_3$. Other cations of smaller radius, such as Rb^+ and K^+ (potassium), cannot form $APbI_3$ structure. However, these cations are demonstrated to be beneficial for the suppression of hysteresis in photovoltaic devices of CsFAMA-triple cation perovskite and contribute to the enhanced thermal stability and photo-stability of perovskite compounds. Saliba *et al.*[86] first developed the quadruple cation system by incorporating Rb^+ as the fourth cation in the RbCsFAMA-quadruple

View Article Online
DOI: 10.1039/C8EE02852D

cation perovskite. In comparison to the CsFAMA-triple cation perovskite, the quadruple cation perovskite exhibited a higher PCE and better thermal stability with a T_{80} of 2500 hours for the MPPT measurement conducted at 85 °C and N_2 atmosphere.(**Figure 4e**) Abdi-Jalebi *et al.*[96] incorporated potassium as the fourth cation into the KCsFAMA-quadruple cation perovskite system. They observed a significant enhancement in the luminescence yields of the perovskite films. In the case of both RbCsFAMA- and KCsFAMA- quadruple cation perovskites, the hysteresis of the devices were considerably suppressed,[97-100] suggesting their impact on ions migration and traps filling.[43]

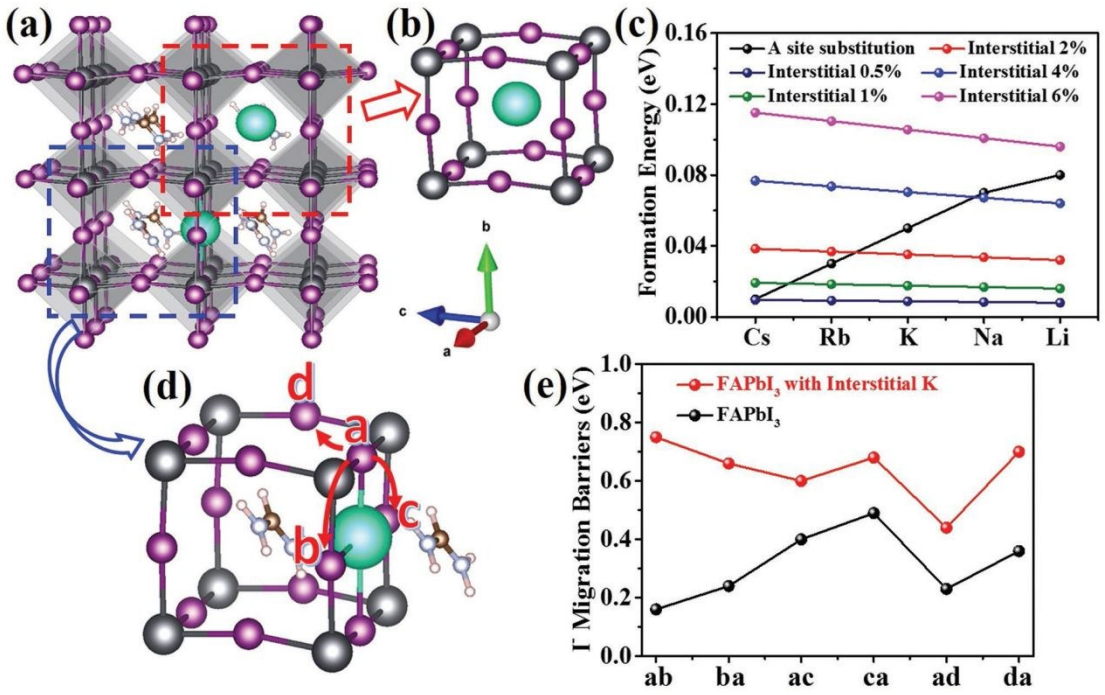

Figure 5. Thermodynamic and kinetic properties of alkali cation incorporation (Cs^+, Rb^+, K^+, Na^+, and Li^+) in $FAPbI_3$. a) Illustration of the possible locations of these cations in $FAPbI_3$: b) at the A site substitution and d) at the interstitial site. c) The formation energy of alkali cation to be at the A site substitution and an interstitial site. d) Illustration of iodide diffusion pathways, using K^+ at an interstitial site of $FAPbI_3$ perovskite as an example. e) Diffusion barriers for iodide migration in $FAPbI_3$ with (red line) and without (black line) interstitial K^+.[100] Reproduced with permission from ref.[100]. Copyright 2018, John Wiley & Sons.

Although the introduction of Rb^+ and K^+ cations into CsFAMA-triple cation perovskite leads to high stability in the compounds and devices, the position of these cations in the crystal structure of perovskite compound is still under debate. A recent study by Cao *et al.*[100] using density functional theory (DFT) showed that Rb^+ could occupy both A site and interstitial site in the ABX_3, as schematically shown in **Figure 5b** and **Figure 5d**, respectively. The formation energy for Rb^+ to be at A site and interstitial sites was about the same, whereas smaller alkali cations, *i.e.* K^+, Na^+, Li^+ were more preferred to be at the interstitial sites. **Figure 5c** shows that

View Article Online
DOI: 10.1039/C8EE02852D

the energy cost of the interstitial occupancy depends on the concentration of the dopants. **Figure 5e** shows the computer calculation results based on DFT that interstitial K^+ cations increased the energy barrier for iodide migration. They were speculated to block the iodide diffusion path, alter the FA^+ cation orientation, and increase the formation energy for iodine vacancy. Blocking iodide migration was found to reduce hysteresis in the device significantly. In good agreement, Son *et al.*[99] calculated that interstitial K^+ cations decreased the electron accumulation and prevented the formation of Frenkel pair defects of iodide, which contributed to the suppression of hysteresis. Furthermore, $MAPbI_3$ with K^+ cation was found to have a lower trap density, which resulted in a great reduction in hysteresis.[99]

However, several recent studies found that Rb^+ and K^+ were segregated at the grain boundaries[96] and surface[101, 102] of the perovskite films. They helped to passivate defects[101-103] and facilitate effective charge transport.[98, 104] Based on the temperature dependent solid-state nuclear magnetic resonance (NMR) result, Kubicki *et al.*[103] discovered a strong interaction between Cs^+ and $[PbI_6]^{4-}$ during temperature variation, implying Cs at the A site of the halide perovskite 3D structure. Also, the depth probe Hard X-ray Photoelectron Spectroscopy (XPS) found Rb^+ had a higher concentration at the surface of perovskite film rather than in bulk.[101, 102] Abdi-Jalebi *et al.*[96] suggested that K^+ cation had an interaction with bromide in the film, particularly surrounding the grains. More specifically, K^+ depleted bromine from the perovskite structure and increased the I/Br ratio inside the bulk of the material. Besides, using KI in the precursor led to an iodide-rich environment before final film formation, which resulted in fewer halide vacancies,[80] reductions in the non-radiative recombination, and suppression in halide migration.[96] Similar results were observed in iodide only perovskites as well.[99, 105]

View Article Online
DOI: 10.1039/C8EE02852D

3.2.4 Inorganic perovskite $CsPbX_3$

i) $CsPbI_3$

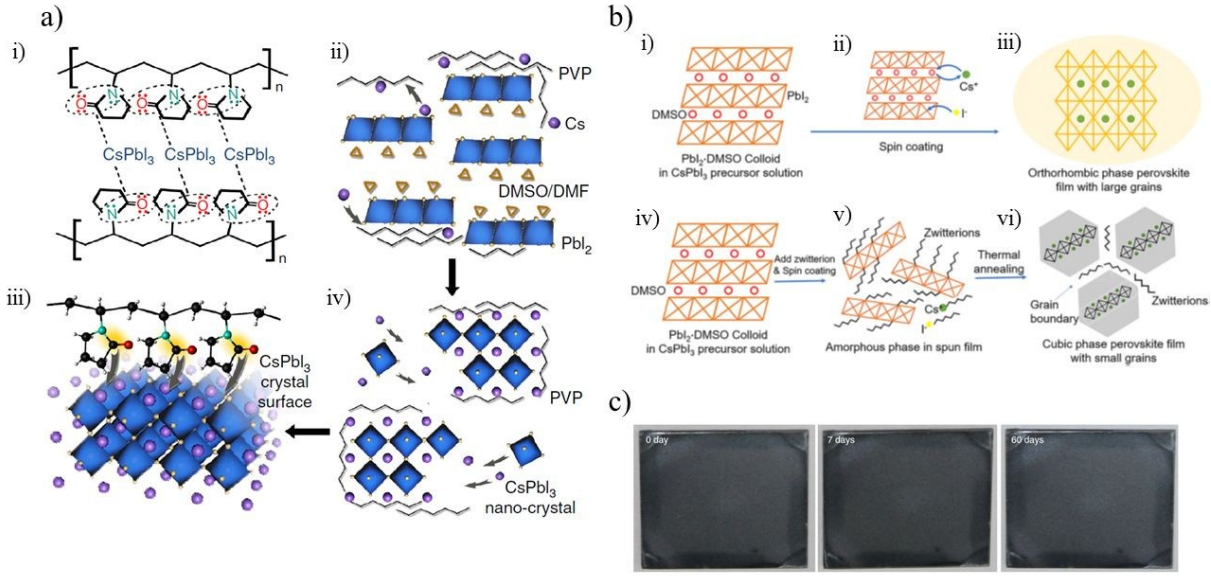

Figure 6. Strategies to stabilise photoactive α- phase $CsPbI_3$. a) Surface passivation *via* PVP:[106] i) interaction of $CsPbI_3$ with acylaminos group in PVP, ii) PbI_2 (blue shape) and Cs (purple ball) assembled around PVP to form metastable state, iii) after the assembling, the $CsPbI_3$ nanocrystals attached around PVP, and iv) PVP at the surface reduced the surface tension of $CsPbI_3$ crystal to stabilise the α-$CsPbI_3$. Reproduced with permission from ref.[106]. CC BY 4.0. b) Reducing crystal sizes by sulfobetaine zwitterion:[107] i-iii) without zwitterion, the δ-phase formed rapidly after spin coating at room temperature, and iv-vi): The zwitterion induced the amorphous phase before annealing, which induced the formation of small nanocrystals of 30 nm with the cubic phase. Reproduced with permission from ref.[107]. Copyright 2018, Elsevier. c) The $CsPbI_3$ perovskite preserved its α-phase in a dry atmosphere for two months, prepared by using solution-controlled growth method to reduce the evaporation rate of the solvent.[108] Reproduced with permission from ref.[108]. CC BY 4.0.

Although the efficiency of PSCs with the state-of-the-art perovskite, *i.e.* CsFAMA-triple cation perovskite has skyrocketed to over 20%,[86] the thermal stability of PSCs at 85 °C - the industrial evaluation temperature for mature photovoltaic technologies - is still very poor, with fast degradation in photovoltaic performance. Part of the reason is due to the decomposition of perovskites that contain organic cations, especially MA^+.[58] In contrast, inorganic perovskite, $CsPb(I_xBr_{1-x})_3$ exhibits excellent thermal stability.[109] In the pioneering work of Eperon *et al.,*[110] they found that although the photovoltaic phase of $CsPbI_3$ was stable in an inert atmosphere at room temperature, moisture exposure transformed the material into non-photoactive δ-phase.[110, 111]

View Article Online
DOI: 10.1039/C8EE02852D

Nonetheless, several strategies have been developed to stabilise the α-phase (cubic phase) of $CsPbI_3$. One example is to mix poly-vinylpyrrolidone (PVP) with $CsPbI_3$ precursor before film deposition. As shown in **Figure 6a**, PVP is proposed to interact with $CsPbI_3$ nuclei, which increases the surface charge, and reduces the surface tension of the $CsPbI_3$ nanocrystals.[106] The non-encapsulated PVP-$CsPbI_3$-PSCs retained 75% of its initial PCE after 500 hours in the ambient air with the relative humidity (RH) at 45-55%. Swarnkar *et al.*[112] used methyl acetate (MeOAc) as a ligand for $CsPbI_3$ quantum dots, which were stable for more than one month in ambient condition. Also, small crystals also stabilise the α-phase of this material. Using the sulfobetaine zwitterion in the perovskite precursor results in 30 nm stable α-$CsPbI_3$ crystals thanks to the hindrance of the formation of δ-phase at room temperature before the annealing step (**Figure 6b**).[107] Devices with this method reached more than 11% efficiency and maintained 85% of the initial efficiency after storage in air for 30 days. Another novel method is to employ 2D perovskite utilising 2.5% bication ethylenediamine cations (EDA^{2+}) in the $CsPbI_3$ system to stabilise its α-phase.[113] The (110) layer of $EDAPbI_4$ acted as a separator of the crystal units and resulted in a nearly 12% efficient device, retaining 80% of its initial efficiency after storage in a dry air box for one month. Recent work by Wang *et al.*[108] demonstrated that high quality and stable α-$CsPbI_3$ films for two months in a dry environment (**Figure 6c**) could be realised by reducing the evaporation rate of the solvent in the precursor (in this case dimethyl sulfoxide). Using this solution-controlled growth method, they reported 14.7% efficiency in $CsPbI_3$ devices.

As regard to the crystal phase of $CsPbI_3$ perovskite at room temperature, more recent works showed that the photovoltaic phase of $CsPbI_3$ at room temperature was an orthorhombic phase or β-phase rather than a cubic phase or α–phase.[114] More interestingly, the titled orthorhombic phase of $CsPbI_3$ perovskite was found to be thermodynamically stable at room temperature. This discovery will help to promote the development of highly stable $CsPbI_3$ devices.

ii) $CsPb(I_xBr_{1-x})_3$

It has been shown that mixing bromide with iodide in the inorganic perovskite $CsPb(I_xBr_{1-x})_3$ can also stabilise the photovoltaic phase of the material. This is possible because bromide of smaller ionic radius extends the tolerance factor for $CsPb(I_xBr_{1-x})_3$ compounds to stay in the cubic crystal structure. Moreover, the commonly used $CsPb(I_xBr_{1-x})_3$ perovskite with the molar ratio of iodide to bromide at 2:1 exhibited good stability against moisture.[115-117] To investigate the influence of bromide on the phase stability of $CsPb(I_xBr_{1-x})_3$ perovskite, our recent work conducted a systematic study on a broad range of bromide content. We found that compounds

View Article Online
DOI: 10.1039/C8EE02852D

with bromide content of at least 40% exhibited strong phase stability during the test for storage in ambient atmosphere for over 100 hours.[118] Compounds with bromide content of less than 40%, in spite of maintaining α-phase in the first ten hours, transformed to δ-phase after storage in ambient atmosphere for 100 hours. By using the stable composition, *i.e.* $CsPb(I_{0.6}Br_{0.4})_3$, our devices achieved over 10% efficiency. In addition to the phase stability, Beal *et al.*[119] studied the photo-induced halide segregation in $CsPb(I_xBr_{1-x})_3$ perovskites. They found that $CsPb(I_xBr_{1-x})_3$ perovskites with $x < 0.4$ showed negligible halide segregation under 1 Sun illumination. The higher tolerance against halide segregation compared to $MAPb(I_xBr_{1-x})_3$ perovskites is due to the low polarizability of Cs^+ at the A site in $APbI_3$, as discussed in section 3.2.1.[76] Yet, ion migration in particular halide migration still exists in $CsPb(I_xBr_{1-x})_3$,[120] which could lead to hysteresis[43] and reversible losses,[121] as reported in the hybrid organic-inorganic perovskite photovoltaics.

iii) $CsPb(I_xBr_{1-x})_3$ of mixed compositions

Considering the tolerance factor, incorporating A^+ site cation of larger ionic radius size and B^+ site cation of the smaller ionic radius can be a route to enhance the phase-stability in inorganic $CsPb(I_xBr_{1-x})_3$ perovskites. Hu *et al.*[122] partially substituted lead with bismuth, which boosted the tolerance factor from 0.81 of α-$CsPbI_3$ to 0.84 of α-$CsPb_{1-y}Bi_yI_3$. This increase in tolerance factor promoted the phase stability. By optimising the ratio, the efficiency of $CsPb_{0.96}Bi_{0.04}I_3$ PSCs reached more than 13% and retained 68% of initial PCE after 168 hours measured in ambient condition (RH ≈ 55%).

View Article Online
DOI: 10.1039/C8EE02852D

3.2.5 2D perovskites and 2D/3D perovskites

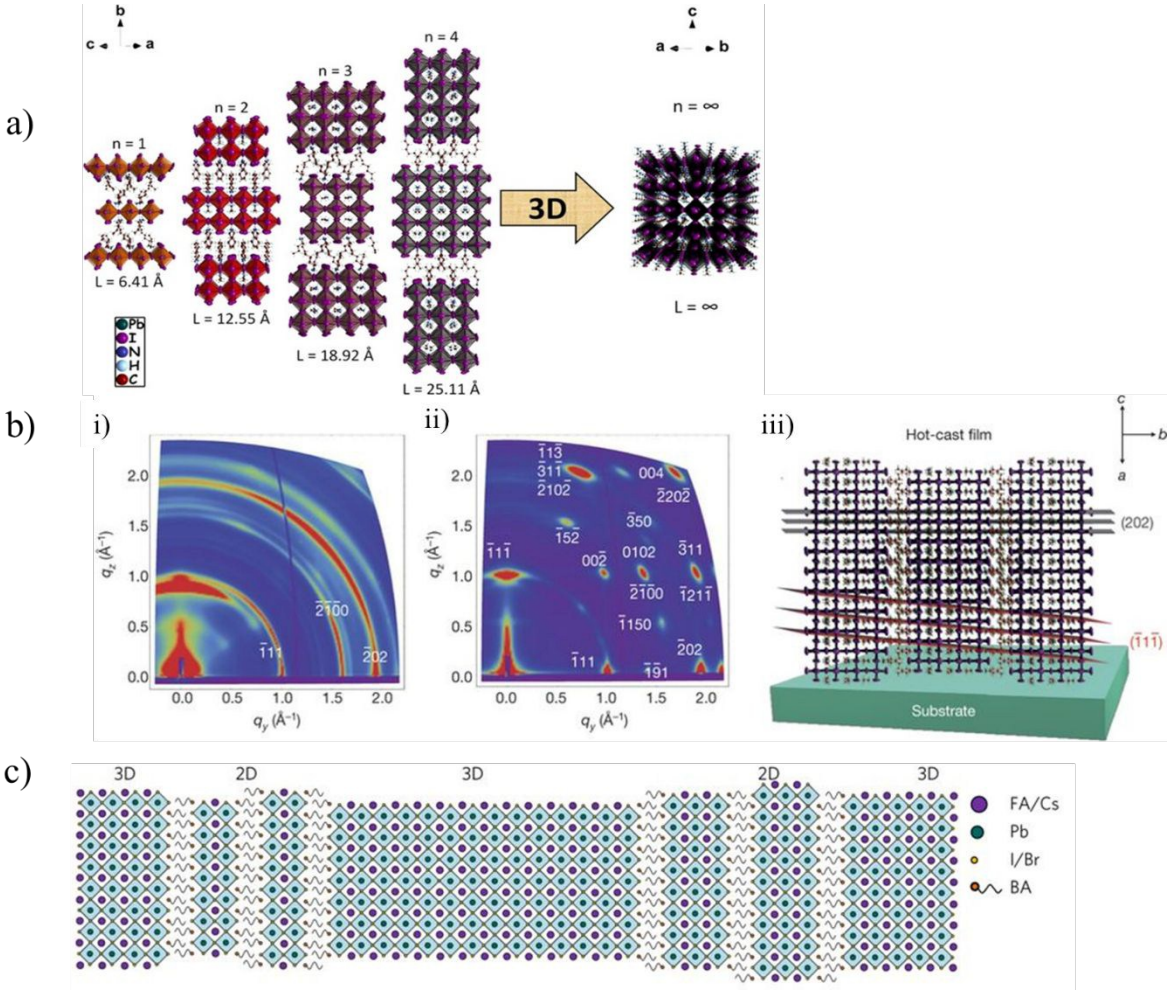

Figure 7. a) Scheme of the crystal structure of $(BA)_2(MA)_{n-1}Pb_nI_{3n+1}$ perovskite family.[83] Reproduced with permission from ref.[83]. Copyright 2016, American Chemical Society. b) GIWAXS maps for i) polycrystalline room-temperature-cast and ii) near-single-crystalline hot-cast $(BA)_2(MA)_3Pb_4I_{13}$ perovskite films and iii) schematic representation of the (101) orientation, along with the $(\bar{1}1\bar{1})$ and (202) planes of a 2D perovskite crystal.[123] Reproduced with permission from ref.[123]. Copyright 2016, Springer Nature. c) Schematic illustration of the proposed self-assembled 2D-3D perovskite film structure.[124] Reproduced with permission from ref.[124]. Copyright 2017, Springer Nature.

In addition to developing resilient 3D perovskite materials, another approach is to employ 2D perovskites. The evolution of 2D perovskites to 3D perovskites is illustrated in **Figure 7a** using an example of $(BA)_2(MA)_{n-1}Pb_nI3_{n+1}$ (BA: n-butylammonium, $C_4H_9NH_3$; n = 1, 2, 3, 4) perovskite family. This type of perovskites was reported by Stoumpos and Cao *et al.*[83], and they found that 2D perovskites exhibited superior moisture stability over 3D $MAPbI_3$ perovskite. The band gap of the layered perovskite family can be tuned from 2.43 eV (n=1), 2.17 eV (n=2), 2.03 eV (n=3), to 1.91 eV (n=4). However, as the value of 'n' increases, it gets difficult to

View Article Online
DOI: 10.1039/C8EE02852D

collect pure 2D perovskite phase. In another work,[125] they applied the 2D perovskite for n=3 compound into solar cells and obtained an initial PCE of 4.02%.

Similarly, Smith *et al.*[126] reported $(PEA)_2(MA)_2[Pb_3I_{10}]$ (PEA: $C_6H_5(CH_2)_2NH_3^+$) perovskite and got a PCE of 4.73%. One reason behind the low efficiency of 2D perovskite devices is the relatively large band gap of the 2D perovskite. The second reason is the non-favoured crystal orientation of 2D perovskite. Ruddlesden-Popper phase layered perovskites, $(RNH_3)_2(A)_{n-1}B_nX_{3n+1}$, where RNH_3 are large alkyl ammonium cations, tend to form a layered structure parallel to the contacts in planar cells. The non-favoured crystal orientation inhibits the charge transport by the large organic cations that act like insulating spacing layered between the conducting inorganic slabs. To solve this problem, Tsai *et al.*[123] developed a hot casting method that resulted in the crystallographic planes of the inorganic perovskite component along (202) facet that had a strongly preferential out-of-plane alignment concerning the contact. The GISAXS (grazing incidence small angle X-ray scattering) measurement showed that the perovskite film behaved similarly to single crystals. (**Figure 7b**) This method helped to promote the PCE to 12.52%. Later, Zhang *et al.*[127] adopted the hot-cast method for 2D perovskite deposition and doped the compound with Cs^+, which led to a PCE of 13.7%. Chen's group developed another method to control the crystal orientation of $(PEA)_2(MA)_{n-1}Pb_nI_{3n+1}$ perovskite.[128] They found that the addition of a small amount of ammonium thiocyanate (NH_4SCN) in the precursor solution resulted in the vertically orientated highly crystalline 2D perovskite using the one-step spin-coating method. In this study, the PCE of $(PEA)_2(MA)_{n-1}Pb_nI_{3n+1}$ PSCs was pushed to 11%.

The device application of another type of layered perovskite, expressed as $(RNH3)_2(MA)_nPb_nI_{3n+2}$ was reported by Wang *et al.*[129] Different from $(RNH_3)_2(MA)_{n-1}Pb_nI_{3n+1}$ perovskites, this type of perovskites exhibited preferred crystal orientation along (002) facet, which indicated the growth of crystals along the Pb_2I_8 inorganic bones. Thus, it provides the chances for efficient charge transport with suppressed influence caused by the long organic cation. Pb_2I_8 perovskite annealed at 100 °C for 15 min leads to a very stable film as characterised by XRD. However, Pb_2I_8 perovskite deposited on TiO_2 planar film exhibited a sever bulk recombination. The employment of TiO_2 mesoporous film showed a significant suppression in the bulk recombination and helped to promote the efficient to over 5%. The relatively low efficiency of the Pb_2I_8 perovskite with the favoured crystal orientation could be partially attributed to the strongly bound excitons that were reported in layered perovskite.[130]

While in early reports, 2D perovskites demonstrated robust stability measured by the UV-Vis and XRD spectroscopy, until recently, the device stability of 2D perovskites has not been fully discussed. This is because of the low efficiency in 2D PSCs and the hysteresis presented in their *JV* scans. Tsai *et al.*[123] examined the stability of their highly efficient 2D perovskite devices by storing them at 1 Sun constant illumination for the photo-stability test and under RH of 65%. They found that, under constant illumination, the efficiency of $MAPbI_3$ perovskite devices with and without encapsulation dropped to 40% of their initial value in approximately 10 hours. In the humidity test, the $MAPbI_3$ devices with and without encapsulation degraded even faster. In contrast, the non-encapsulated 2D perovskite devices maintained 60% of their initial value, while no degradation in efficiency was observed in the encapsulated 2D perovskite devices for over 2000 hours constant illumination.

Rational design of 2D/3D heterostructured perovskites demonstrated a successful mixture of 2D and 3D perovskites. Wang *et al.*[124] introduced BA^+ cation into $BA_x(FA_{0.83}Cs_{0.417})_{1-x}Pb(I_{0.6}Br_{0.4})_3$ perovskite. (**Figure 7c**)They found that the ratio between the long organic cation (BA^+) and small cations (FA^+, Cs^+) had a significant influence on the final morphology of the perovskite films. The large presence of BA^+ cation in the compound led to plate-like crystals in the film. Moreover, they conducted a quantitative analysis of the device stability by fitting the post "burn-in" section of the PCE to a straight line and extrapolated the curve back to zero time. They calculated that T_{80} was 1005 h for 2D/3D mixed devices, which was about 1.5 times that of FACs-double cation devices.

3.3 Hole selective materials (HSMs)

HSMs are key constituents of high-performance PSCs, since they ensure an efficient charge extraction from the perovskite layer, and prevent the direct contact between perovskite and the metal electrode in regular structured devices. HSMs are also intrinsically affecting device stability of PSCs. Designing low-cost, efficient, and stable HSMs represents a challenge to be urgently addressed.[131]

3.3.1 Inorganic HSMs

The choice of inorganic HSMs is restricted to good energetic interfacing to halide perovskites. Narrowing down to the state-of-the-art halide perovskite compositions, *i.e.* $MAPbI_3$ and CsFAMA, this criterion translates into a valence band level close to -5.4eV.[132-134] A deeper valence band would result in an energetic barrier for hole extraction, while a shallower one would decrease the device built-in potential impacting surface recombination.[135]

View Article Online
DOI: 10.1039/C8EE02852D

Among eligible materials there are binary transition metal oxides (NiO_x, CuO_x, CrO_x, CoO_x), tertiary oxides ($LiCoO_2$, $NiCoO_4$, delafossite p-type TCO), and copper-based materials (CuI and CuSCN).[136, 137] Graphene-like (2D) materials, such as graphene oxide (GO), reduced GO (rGO), and MoS_2 have been reported as excellent anodic interlayers. Extended application of inorganic HSMs in n-i-p architecture is still limited by obvious difficulties in processing these materials on top of perovskite layers, due to solvents or processing temperature incompatibility. Therefore, p-i-n architecture remains the platform of choice for testing implementation of inorganic HSMs, with efficiencies now competitive with n-i-p architecture.[138, 139]

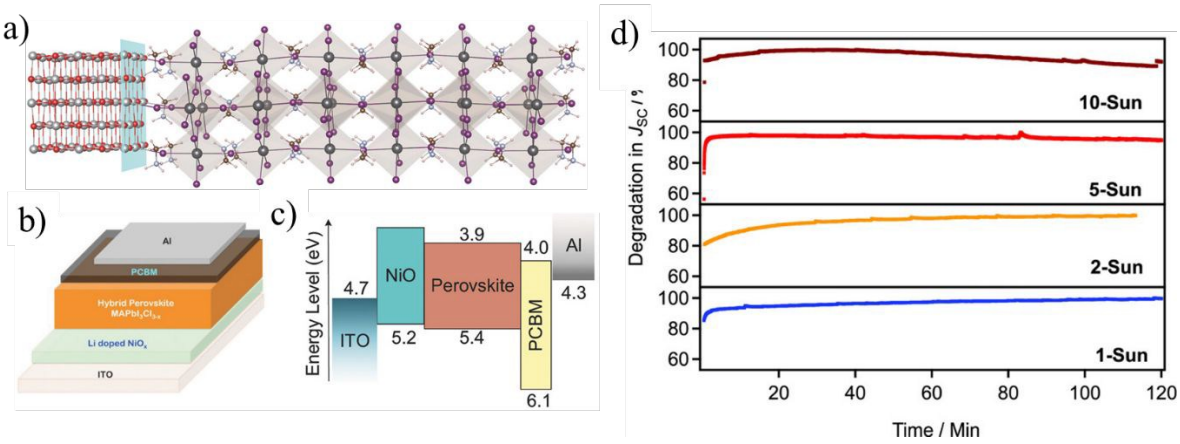

Figure 8. a) Ni─I bonds at the interface region of $NiO/MAPbI_3$ calculated from DFT. (red sphere stands for O, grey for Ni, purple for I, light blue for N, brown for C, and pink for H). b) Scheme for Li-NiO based p-i-n structured devices. c) Energy diagram for each component in the device and d) J_{sc} time evolution of $MAPbI_3$/LiNiO device measured at different light intensities.[140] Reproduced with permission from ref.[140]. Copyright 2017, John Wiley and Sons.

i) Interface chemical stability

The primary requirement for choosing a selective contact is its chemical compatibility with metal halide perovskite. Generally, the p-type conductivity of inorganic materials is associated with their defect chemistry and the consequent mixture of oxidation states into the crystal lattice.[141] This characteristic makes these materials chemically and electrochemically reactive. We believe that more efforts are needed to understand the interfacial chemistry at the HSM/perovskite interface. It is experimentally challenging given the nature of *buried interface* in p-i-n PSCs. Computer simulation represents a powerful tool to gain insights into this buried interface. An oxygen-rich $MAPbI_{3-2x}O_x$ phase has been suggested through simulation, and also evidenced from XPS depth profiling investigation at $MAPbI_3$/NiO.[142, 140] More recently the occurrence of Ni-I bonds was calculated,[140] (**Figure 8a**). Similar Ti-I-Pb bonds were reported at the $TiO_2/MAPbI_3$ interface.[143, 144] This kind of interfacial interactions could affect surface

charge accumulation that could induce hysteresis and jeopardise stability.[145, 146] A detailed investigation through XPS analysis on films with thickness ranging from 1.5 Å to few nanometres found Mo^{4+} at the interface between $CH_3NH_3PbI_3$ and MoO_x,[147] although the native electronic structure of MoO_x is constituted by Mo^{6+} and Mo^{5+} oxidation states. The formation of MoO_2 at $MAPbI_3/MoO_3$ interface negatively affected device operation and a chemical decoupling through a Spiro-OMeTAD interlayer ($MAPbI_3$/Spiro-OMeTAD/MoO_3) was needed to overcome the occurrence of interfacial redox. Acik *et al.*[148] investigated chemistry reaction at the interface of GO and perovskite precursor solution. They reported a chemical reduction of GO through halides. The process affected the properties of GO as substrates for halide perovskite growth and lead to possibly detrimental oxygen-induced defects at the GO/perovskite interface. Understanding these interactions is an essential condition for the advancement of research in halide perovskite photovoltaics, and can reveal otherwise hidden degradation mechanisms.

ii) Photo-stability

Back in 2015, Chen *et al.*[149] reported Li^+, Mg^{2+} co-doped NiO HSM in p-i-n structured PSCs that retained 90% of their initial efficiency after constant illumination at AM1.5G one sun for 1000 h. The introduction of foreign atoms, usually in atomic percentage range between 0.1 ~ 10%, does not only affect the optoelectronic properties of the inorganic semiconductor, but also influences its crystallinity, morphology (*i.e.* surface roughness), and its surface energy. The influence of foreign atoms is more crucial in p-i-n device architecture as the bottom inorganic HSM affects the film formation and quality of halide perovskite. Nie *et al.*[140] deposited $MAPbI_3$ on lithium doped NiO (Li:NiO), and observed a superior crystallinity and micro-strain reduction in perovskite film compared to that of PEDOT:PSS. The scheme of device architecture and energy alignment among components of the device are given in **Figure 8b-c**. Their devices showed robust photostability for continuous illumination at high light intensities of up to 10 Sun (**Figure 8d**). Also, V_{oc} of their devices reaches a stabilised value extremely fast in less than one second, while usually it is observed that V_{oc} of PSCs increases in the first few minutes and then become stabilised. The light-soaking induced increase in V_{oc} recently has been correlated to a strain reduction in perovskite crystal structure,[150] and the chemical interaction between surface halide in perovskite film and fullerene at the cathode.[151, 152]

Another strategy is to reduce the UV-light soaking for perovskite. In p-i-n architecture, this can be realised by employing an HSM of the relatively narrow bandgap. Hua *et al.*[153] introduced delafossite-type $CuCrO_2$ into $MAPbI_3$ p-i-n structured devices that showed high hole mobility

View Article Online
DOI: 10.1039/C8EE02852D

of 10 $cm^2V^{-1}s^{-1}$ that was two orders of magnitude higher than NiO (0.1 $cm^2V^{-1}s^{-1}$), leading to improved hole extraction and transport, and an increase in FF and V_{oc}. More importantly, the relative low band gap (2.9 eV) of $CuCrO_2$ shielded $MAPbI_3$ from UV-light, leading to strongly improved long-term stability under UV exposure. After 300 h of UV-light exposure, they observed the feature peak of PbI_2 in XRD measurement of NiO based devices, and a significant decrease in J_{sc}. In contrast, they found that $CuCrO_2$ based devices maintained over 90% of the initial value after 1000 h illumination under UV light.

iii) Thermal stability

The accelerated ageing test has been a popular tool for evaluating the lifetime of silicon solar cells and polymer solar cells. It requires measuring the devices at an elevated temperature, such as 85 ^{0}C. Islam *et al.*[154] studied the acceleration factor, *K*, of 15% efficiency NiO/$MAPbI_3$/PCBM/AZO/Ag devices, under the assumption of an Arrhenius model, defined by the equation:

$$K = \exp\left[\frac{E_a}{k_B}\left(\frac{1}{T_{high}} - \frac{1}{T_{low}}\right)\right] \qquad \text{Eq.2}$$

where E_a is the activation energy for the degradation processes in electron volts (eV), k_B is the Boltzmann constant. By measuring the MPPT for 1000 h at two temperatures, 30°C and 85°C, they estimated the activation energy to be around 0.3 eV, which is similar to the value obtained for polymer solar cells.[155] The value of activation energy adopted from Arrhenius model is highly dependent on the materials. It relates to the morphology change or composition change at elevated temperatures. Chiang *et al.*[156] observed negligible loss after five days at 60°C for $LiCoO_2$ HSM, but their devices started to degrade at over 90°C, which was largely due to the low thermal stability of the $MAPbI_3$ perovskite. In both studies, the authors compared the device stability with PEDOT:PSS-based devices and found superior stability in inorganic HSMs-based devices. Ouyang *et al.*[157] employed low temperature processed $NiCo_2O_4$ of high hole mobility in p-i-n architecture. This material achieved an efficiency of over 18%, which is highly competitive for NiO. Remarkably, the devices without encapsulation retained over 90% in MPPT measurement for 500 h under AM 1.5 G 1 Sun illumination in ambient condition.

Limited studies have been reported employing inorganic HSCs in n-i-p structured devices. One pioneering work in this field is conducted by Arora *et al.*,[158] who applied CuSCN in n-i-p devices. Surprisingly, CuSCN spin coated from diethyl sulphide did not bring noticeable damage to the beneath perovskite film. Rather, they found that rGO interlayer was critical for CuSCN/Au interface to avoid oxidisation of gold by thiocyanate anions under the influence of

View Article Online
DOI: 10.1039/C8EE02852D

light. Amazingly, their devices maintained 95% of initial efficiency after 1000 h MPPT measurement at 60 °C in the N_2 atmosphere. Besides, few works employed NiO nanoparticles ink as a route to deposit inorganic HSC in n-i-p structured devices.[159] Yet the efficiency is far lagged behind that of p-i-n structured devices.

iv) Reverse bias stability

In one recent work conducted by Bowring *et al.*,[160] discussed the reverse bias stability of devices ITO/NiO/CsFAMA perovskite/C_{60}/SnO_2/ITO. They found that shaded cells in the module were put into reverse bias by the illuminated cells, which was most likely due to tunnelling mediated by mobile ions. During this process, series resistance increased while V_{oc} decreased. Infrequent random shading, such as from clouds could not be an issue. However, daily shading caused by a tree or other nearby stationary objects could create a serious pathway to device degradation for residential application. Rajagopal *et al.*[161] reported that a similar phenomenon was specific of NiO/$MAPbI_3$ interface yet not observed at the presence of PEDOT:PSS interlayer between NiO and perovskite. The authors believed that the reverse bias behaviour was attributed to the formation of a transient tunnel junction at NiO/$MAPbI_3$ interface. More efforts in this regard are needed to examine the reverse bias stability of devices of different architectures and components.

View Article Online
DOI: 10.1039/C8EE02852D

3.3.2 Organic HSMs

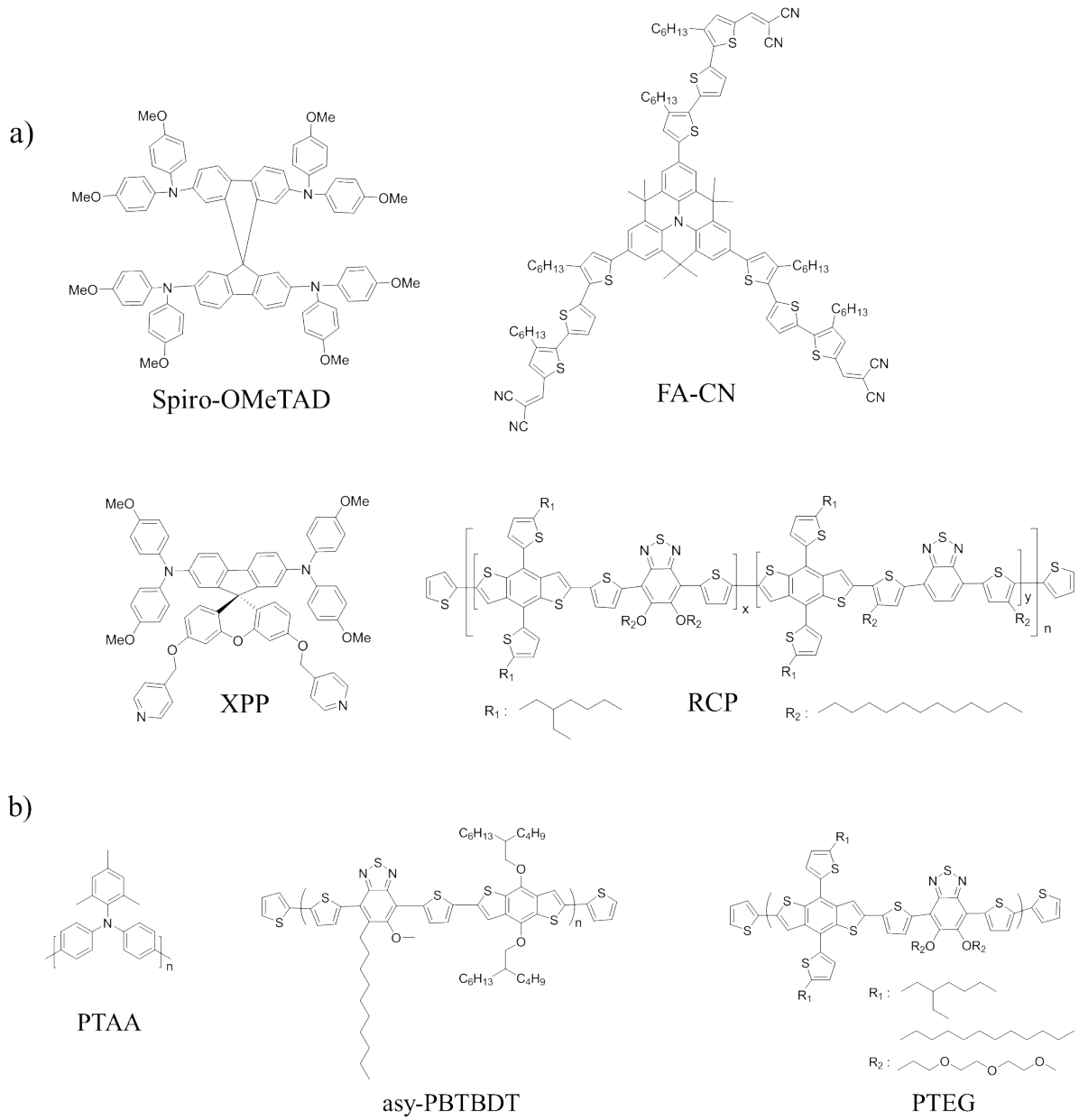

Figure 9. Key examples of a) small molecules and b) polymeric HSMs for highly efficient and stable PSCs. The structures of the two most common reference materials, Spiro-OMeTAD (small molecule) and PTAA (polymer), are also included in a) and b).

i) Instability in organic HSMs

Most of the state-of-the-art HSMs rely on organic small-molecules and polymers. Small molecules, having distinct structure and molecular weight, are the best option when high purity and yields are desired in industrial production.[95] On the other hand, polymeric HSMs are preferred for their relatively good thermal and mechanical stability, the higher hole mobility, and easy processing. **Figure 9** illustrates the molecular structure of the most commonly used organic HSMs in PSCs. Typically, organic HSMs are based on a triphenylamine (TPA) moiety,

due to the presence of electron-rich nitrogen atom, which minimises the intermolecular distance leading to non-planarity of the TPA system. This ultimately results in the formation of amorphous materials, a beneficial feature for HSMs to ensure a good electronic contact to the perovskite surface.[162] Among the small molecules, 2,20,7,70-tetrakis-(N,N-di-p-methoxyphenylamine)-9,90-bifluorene (Spiro-OMeTAD) is a TPA-based HSM adopted in the great majority of the works first on solid-state DSSCs[163] and later on PSCs as well because the PSCs efficiencies achieved with it have been rarely attained or exceeded with other small molecules. As for the polymeric HSMs, poly-[bis(4-phenyl)(2,4,6-trimethylphenyl)amine] (PTAA) was the first one tested in PSCs and still the material leading to the champion PSCs with world record efficiency.[164] However, these two materials are far from being the optimal choice. Both are prohibitively expensive (~300 $/g for Spiro-OMeTAD and 1903.5 $/g for PTAA)[95, 165] because of their onerous multistep synthetic schemes and the costly purification steps.[166]

Moreover, pristine Spiro-OMeTAD, as most of the organic HSMs, shows modest hole mobility and conductivity (1.67 x 10^{-5} cm^2 V^{-1} s^{-1} and 3.54 x 10^{-7} S cm^{-1}, respectively),[167] thus requiring chemical p-dopants to enhance the hole conductivity and thus the efficiency of PSCs. Commonly, lithium bis(trifluoromethanesulfonyl) imide salt (LiTFSI) and 4-*tert*-butylpyridine (tBP) are used as dopants with Spiro-OMeTAD and PTAA as well, to enhance the photovoltaic performance.[168] When comparing the electrical *JV* and impedance spectroscopy responses of PSCs based on small molecule (Spiro-OMeTAD) or polymeric HSMs (poly(3-hexylthiophene 2,5-diyl), P3HT) with and without chemical doping, Ulfa *et al.*[169] found out that the effect of doping on the performance has much higher weight in case of small molecular HSMs. The PSCs performance is limited by the HSM layer resistance and by the charge recombination at the HSM/perovskite interface. However, the presence of a hydrophilic dopant, namely, LiTFSI accelerates the degradation in the photovoltaic performance of devices.[170] Thus it is not a preferred choice when aiming to highly stable devices. Besides the negative influence caused by the dopant, a low glass transition point in HSMs will lead to poor thermal stability of PSCs in the accelerated ageing test.[162] In the following, we will give a few examples of dopant-free HSMs and discuss the thermal stability of HSMs and their influence on device stability.

ii) Dopant-free HSMs

Table 1. Summary of the most efficient dopant-free organic HSMs reported in the literature.

Key moieties or composition	Advantages	Code	Efficiency	Stability	Ref.
D-π-A: Triazatruxene donor-thiophene-based multiple conjugated arms and malonitrile acceptor	Face-on stacking organization on perovskite, which favors vertical charge carrier transport	KR321	19%	60% v.s. 20% of initial PCE for KR312 and spiro-OMeTAD after 650 h constant illumination in N_2 atmosphere.	171
D-π-A: A rigid quinolizino acridine and a flexible triphenylamine donors with akyl-substituted terthiophene, and malononitrile as electron acceptor	Suitable HOMO level and high intrinsic hole mobility	FA-CN and TPA-CN	18.9 % (FA-CN) 17.5% (TPA-CN)	65% v.s. 15% of initial PCE for FA-CN and spiro-OMeTAD after 1300 h constant illumination in N_2 atmosphere.	171
2D discotic anthanthrone (ANT) core HSMs end capped with methoxy TPA at both ends (TPA-ANT-TPA and ACEANT-ACE)	Formation of a fully homogeneous protective coating HSM film on the surface of perovskite	TPA-ANT-TPA	17.5%	80% v.s. 14% of initial PCE for TPA-ANT-TPA and Spiro-OMeTAD after 200 h of continuous 1 Sun illumination in ambient air	172
3D HSMs based on spiro-fluorene derivative, in which pyridine group has been pendant to respective HSMs with different positions of nitrogen atoms (*para*, *ortho* and *meta* substitution)	The functionalization with pyridine moiety is responsible for much better long-term stability than traditional HSM wit tBP dopant.	XDB, XOP, XMP, and XPP	17.2% (XPP without Tbp), 19.5% (XPP)	70% after 45 days v.s. 30% after 15 days for XPP and Spiro-OMeTAD non-encapsulated devices stored under ambient air with RH of 40~50%.	173
dopant-free 1D materials tetrathiafulvalene derivative	The intermolecular π–π stacking and chalcogen interactions between TTF derivatives remove the need of dopants	TTF-1	11%	A 20% decrease in PCE after 360 h (TTF-1) v.s. 120 h (spiro-OMeTAD)	174
1D linear molecular D'−A−D−A−D−A−D'-type HSM, based on monofluoro-substituted benzothiadiazole (FBT) and substituted silolodithiophene (DTS)	Good hydrophobicity, arising from the extended π-structure with small intermolecular spaces that impede moisture intrusion.	DFBT(DTS-FBTTh$_2$)$_2$	17.3%	80% was retained after over 500 h in high humidity (RH= 60%) with 1 sun light-soaking.	175
polymeric dopant-free HSMs employ BDT and FBT groups	Hydrophobic material with high hole mobility and deep HOMO level	RCP	17.3%	17.3% for over 1400 h at RH of 75% for storage in darkness at room temperature.	176
polymeric HSM is the D-A type also based on BDT and FBT groups, but with asymmetric alkyl substituents on FBT units instead of the conventional symmetric alkyl substitution	Soluble in green solvents, such as 2-methylanisole	asy-PBTBDT	18.3%	91% was retained after storing the non-encapsulated devices for 30 days in RH of 50~75%.	177
D-π-A conducting homopolymer comprising the usual BDT and FBT moieties with addition of tetraethylene glycol (TEG)	Deep HOMO and good contact between perovskite and this HSM ensures effective hole transfer	PTEG	19.8%	98% for PTEG v.s. 85% for spiro-OMeTAD after 200 h, RH 25%, room temperature, in air.	178

A rich variety of organic materials have been proposed to replace Spiro-OMeTAD and other dopant-based HSMs, to improve the moisture resiliency and the overall PSCs stability.[171, 179-182] Such dopant-free HSMs have a good charge transport characteristic in pristine form and appropriate energy levels to avoid the additional requirement for doping to achieve an efficient charge extraction.

Table 1 summarises the most representative recent examples of organic dopant-free HSMs, leading to the highest performance of the corresponding PSCs regarding efficiencies and stability. It is worth noting that a fair comparison between the HSMs is difficult, especially considering the lack of standard and widely adopted testing protocols for characterising PSCs and assessing their stability.[33, 183]

Another strategy to enhance the HSM transport properties without recurring to dopants consists in the partial pre-oxidizing of the HSM. Nguyen *et al*. demonstrated how to remarkably increase the overall conductivity of HSM after pre-oxidation of a small fraction of Spiro-OMeTAD. The corresponding devices had comparable performances to devices with conventional Li-TFSI doping but had more stable performance under illumination.[184] Leijtens *et al*. applied the same technique to a range of other molecular HSMs, demonstrating improved charge transport characteristics after partial pre-oxidation.[185]

iii) Thermally stable HSMs

Organic HSMs intrinsically affect also the thermal stability of PSCs, even more than the actual hybrid perovskite layer. Small molecules HSMs tend to crystallise at relatively low temperature, thus weakening the contact with the perovskite and the metal electrode, which in turn worsens the PSCs performance. Spiro-OMeTAD is not stable at temperatures higher than 100 ^{0}C since crystallisation onsets at this temperature.[162] Larger crystals within the amorphous Spiro-OMeTAD cause morphological hole traps, thus affecting the charge transport. Moreover, dopants also reduce the glass transition temperature of Spiro-OMeTAD, thus accelerating its crystallisation.[186] Hence, replacing Spiro-OMeTAD with thermally stable materials with high mobility to enhance the fill factor is paramount.[187]

Polymeric HSMs are thermally more stable than their molecular counterparts, because of the lower tendency of polymers to crystallise during the whole operating temperature range of solar cells.[131] The metal electrode (typically gold) migration across the HSMs into the perovskite layer at moderate temperature (70 ^{0}C) is the dominant factor in severe performance losses and has to be blocked. Some approaches to hinder gold diffusion in PSCs include the deposition of buffer layers based on alumina nanoparticles or the introduction of chromium interlayers.[170, 188,

View Article Online
DOI: 10.1039/C8EE02852D

[189] The above mentioned inherent stability towards crystallisation of polymeric HSMs makes them a good barrier to the gold migration,[24, 86, 188, 190] with excellent results regarding stability within the working temperature range of solar cells. PTAA was successfully adopted even at 85 ^{0}C in a stable device based on RbCsFAMA perovskite that retained 95 % of its initial efficiency after 500 h under full illumination and MPPT.[86]

3.4 Electrode materials

In both regular structured PSCs and inverted structured PSCs, metals, such as gold, silver, copper or aluminium are deposited on top of the device for charge collection. These metal contacts, in general, have a deep work function that is beneficial for a high photovoltage in PSCs.[191] Several works suggested that an ohmic contact was formed at the interface between gold and HSM, like Spiro-OMeTAD,[192] which benefits the efficient charge collection to the metal contact. Moreover, the metal contact reflects light and thus enhances the light capture of the system.[193] However, silver, copper and aluminium can be easily oxidised in ambient air. The formed metal oxide layer is an insulating layer that contributes to the serial resistance of the device, and to an extent, it can bring significant drops in the photovoltaic performance of PSCs. Compared to silver, copper and aluminium, gold is more chemically inert, and the bulk of gold will maintain its metallic property even though the very top thin surface (limit to few nanometres) may have some oxidation. As a result, gold, though it is expensive, seems to be an ideal contact for the stable devices. However, several studies found that gold metal contact is not good for the long-term stability of PSCs. First, gold can diffuse through the HSC and reacts with halides in perovskite film forming a metal halide barrier layer that significantly reduces the photovoltaic performance of the device.[188] Similar or even worse condition are observed for silver and copper.[194] Secondly, halide migration in perovskite films can move through the HSC and reach the metal contact, which leads to degradation in efficiency as well.[195] Direct observation of the two processes has been reported.[196]

An interlayer between the gold and HSCs can help to avoid the formation of metal halide. Domanski *et al.*[188] deposited a thin layer of chromium between the gold contact and HSC because chromium is chemically inert to halides and has a high atomic density to prevent gold diffusion. In the ageing test, they conducted the MPPT under 1 Sun illumination at 75 °C and N_2 flow for 12 hours. At the first one or two hours, devices with and without Cr both showed an exponential decay. After that, PSCs with Cr interlayer stabilised at 83% of the initial PCE value. In contrast, PSCs without Cr interlayer exhibited a linear decrease as the time goes, and lost over 50% of its initial efficiency after 12 hours illumination. Beside Cr interlayer, Al_2O_3

View Article Online
DOI: 10.1039/C8EE02852D

was also examined as the interlayer between HSC and gold. It also helped to enhance the device stability.

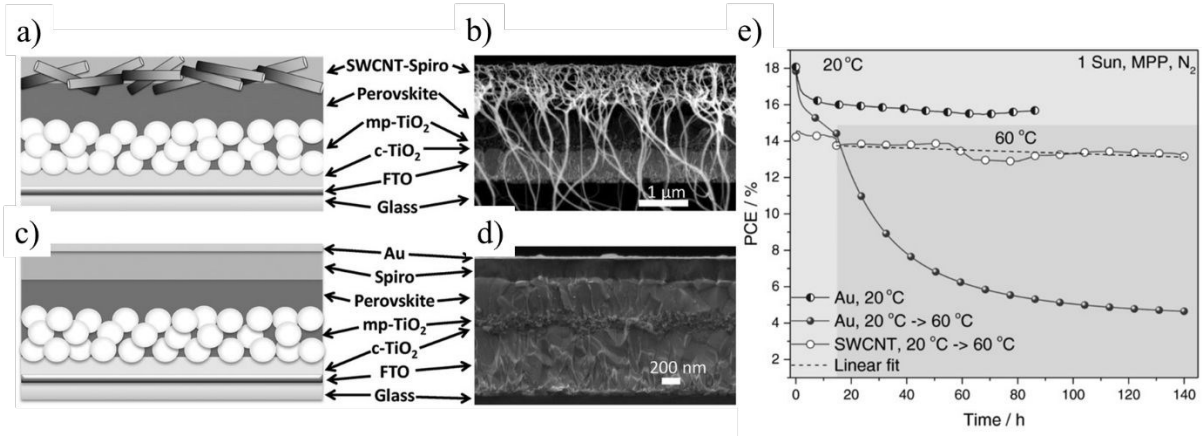

Figure 10. Schemes of device architectures a) without and c) with Au metal contact and the corresponding SEM images in b) and d).[197] e) Comparison of the MPPT results of PSCs using Au and SWCNT as contacts at elevated temperatures Reproduced with permission from ref.[197]. Copyright 2017, John Wiley and Sons.

Another method is to replace gold with some materials that are chemically inert to halides, such as carbon.[198] Indeed, carbon is a popular yet cheap and stable electrode material with adjustable work junction.[199, 200] Several studies reported carbon black and carbon nanotubes as the electrode material.[199] Aitola *et al.*[197] reported a metal-free PSC with HSC based on press-transferred single-walled carbon nanotube (SWCNT) film infiltrated with Spiro-OMeTAD. The device architecture is displayed in **Figure 10a-d**. Amazingly, a PCE of over 16% was achieved with SWCNT-based PSCs without the use of costly metal electrodes. They conducted the MPPT measurement of the devices with and without gold contact for 140 hours under white LED illumination with an intensity equivalent to 1 Sun in the N_2 atmosphere. (**Figure 10e**) The temperature was raised from 20 °C to 60 °C after the first 14 hours of light soaking. In this experiment, they observed a fast degradation in gold contained PSCs, with the efficiency, dropped to less than 80% of its initial value in the first 20 hours, while PSCs using SWCNT/Carbon hold over 90% of its initial value for 140 hours. The authors calculated the value of T_{80} was 580 h for this type of solar cells based on the assumption that the degradation trend would continue after 140 hours.

4. Prospects and Conclusions

Based on the above discussion, we believe that all inorganic PSCs will clear the hurdle of a short lifetime in PSCs on the path to commercialisation. However, the development of all inorganic PSCs is lagged behind the organic-inorganic hybrid PSCs. Part of the reason is that

the all inorganic $CsPbI_3$ perovskite needs high-temperature annealing and the deposition techniques developed for organic-inorganic perovskites cannot be directly adapted to all inorganic perovskites. Another important reason is that the cubic-phase $CsPbI_3$ perovskite is thermodynamically non-stable at room temperature, but rather it transforms into a non-photovoltaic phase (δ-phase).[114] The reason behind this is the small ionic radius of Cs^+ that results in a high lattice strain in the $APbI_3$ crystal to hold the cubic-phase at room temperature.[201] Partially replacing iodide with the smaller sized bromide helps to stabilise its crystal structure. Indeed, it is reported that Br-mixed $CsPbI_3$ shows a stable cubic phase yet leads to a higher optical band gap. The most commonly used $CsPbI_2Br$ perovskite has an optical band gap of around 1.92 eV that is not favourable for either single junction solar cells or tandem cells. The recent work by Sutton *et al*.[114] showed that the fast quenching of $CsPbI_3$ perovskite from 300 °C would result in a room-temperature stable orthorhombic phase or β-phase that is also a photovoltaic phase. Meanwhile, $CsPbX_3$ (X=I/Br/Cl) quantum dots have been synthesised, and they showed excellent stability in photovoltaic application.[202]

Despite the challenges in the field of inorganic PSCs, several recent works have demonstrated efficiencies of over 10% for inorganic PSCs.[116, 203-205] More interestingly, if we take a closer look at these works, we will notice that two trends are developed in this field. One trend is to develop versatile solution-processed methods to deposit a smooth and compact $CsPbX_3$ (X= I/Br) perovskite film.[116, 205] The other trend is to dope $CsPbI_3$ with foreign atoms, such as Eu^{2+}.[202, 206] Yet, it is also noticed that the method developed for mixed halide inorganic perovskite may not give a good perovskite film for $CsPbI_3$ perovskite. To better process the inorganic perovskite film, we need to have a better understanding of the crystallisation process of inorganic perovskite out of solution.

Furthermore, the knowledge on selective contacts developed for organic-inorganic perovskites should be used to instruct the device structure of all inorganic PSCs. Up to now, we have seen that inorganic PSCs exhibited robust stability in the accelerated ageing test.[203] To further promote the development of the lifespan in PSCs, and to make the data reported by different research groups comparable with each other, it is highly important to establish a unified protocol for ageing test of PSCs. As we discussed in Section 2, the testing protocol should consider several factors, including the hysteresis, the "burn-in" period, and the "reversible losses or gain" in PSCs. When the lifespan of PSCs are reported in one work, more than one sample should be tested, and detailed testing conditions should be provided at least in the supporting information. A unified protocol for ageing test will help to set a standard evaluation

process of PSCs, which will benefit the industrialisation of this young photovoltaic technology shortly.

Conflicts of interest

There are no conflicts to declare.

References

1. L. M. Herz, *ACS Energy Letters*, 2017, **2**, 1539-1548.
2. Y. Kanemitsu, *Journal of Materials Chemistry C*, 2017, **5**, 3427-3437.
3. J. Maes, L. Balcaen, E. Drijvers, Q. Zhao, J. De Roo, A. Vantomme, F. Vanhaecke, P. Geiregat and Z. Hens, *The Journal of Physical Chemistry Letters*, 2018, **9**, 3093-3097.
4. S. De Wolf, J. Holovsky, S.-J. Moon, P. Löper, B. Niesen, M. Ledinsky, F.-J. Haug, J.-H. Yum and C. Ballif, *The Journal of Physical Chemistry Letters*, 2014, **5**, 1035-1039.
5. N.-G. Park, *Materials Today*, 2015, **18**, 65-72.
6. M. Lyu, M. Zhang, N. A. Cooling, Y. Jiao, Q. Wang, J.-H. Yun, B. Vaughan, G. Triani, P. Evans, X. Zhou, K. Feron, A. Du, P. Dastoor and L. Wang, *Science Bulletin*, 2016, **61**, 1558-1562.
7. Y. Ogomi, A. Morita, S. Tsukamoto, T. Saitho, N. Fujikawa, Q. Shen, T. Toyoda, K. Yoshino, S. S. Pandey, T. Ma and S. Hayase, *The Journal of Physical Chemistry Letters*, 2014, **5**, 1004-1011.
8. J. Kang and L.-W. Wang, *The Journal of Physical Chemistry Letters*, 2017, **8**, 489-493.
9. A. Miyata, A. Mitioglu, P. Plochocka, O. Portugall, J. T.-W. Wang, S. D. Stranks, H. J. Snaith and R. J. Nicholas, *Nature Physics*, 2015, **11**, 582.
10. Q. Wang, M. Lyu, M. Zhang, J.-H. Yun and L. Wang, *Journal of Materials Chemistry A*, 2017, **5**, 902-909.
11. L. Zhang, X. Yang, Q. Jiang, P. Wang, Z. Yin, X. Zhang, H. Tan, Y. Yang, M. Wei, B. R. Sutherland, E. H. Sargent and J. You, *Nature Communications*, 2017, **8**, 15640.
12. M. I. Saidaminov, V. Adinolfi, R. Comin, A. L. Abdelhady, W. Peng, I. Dursun, M. Yuan, S. Hoogland, E. H. Sargent and O. M. Bakr, *Nature Communications*, 2015, **6**, 8724.
13. N. Tripathi, M. Yanagida, Y. Shirai, T. Masuda, L. Han and K. Miyano, *Journal of Materials Chemistry A*, 2015, **3**, 12081-12088.
14. W. Qiong, C. Hongjun, M. Eric and W. Lianzhou, *Advanced Energy Materials*, 2015, **5**, 1501418.
15. J. Ávila, C. Momblona, P. P. Boix, M. Sessolo and H. J. Bolink, *Joule*, 2017, **1**, 431-442.
16. N. J. Jeon, J. H. Noh, Y. C. Kim, W. S. Yang, S. Ryu and S. I. Seok, *Nature Materials*, 2014, **13**, 897.
17. T.-B. Song, Q. Chen, H. Zhou, C. Jiang, H.-H. Wang, Y. Yang, Y. Liu, J. You and Y. Yang, *Journal of Materials Chemistry A*, 2015, **3**, 9032-9050.
18. M. Xiao, F. Huang, W. Huang, Y. Dkhissi, Y. Zhu, J. Etheridge, A. Gray-Weale, U. Bach, Y.-B. Cheng and L. Spiccia, *Angewandte Chemie*, 2014, **126**, 10056-10061.
19. J.-W. Lee and N.-G. Park, *MRS Bulletin*, 2015, **40**, 654-659.
20. B. R. Sutherland, S. Hoogland, M. M. Adachi, P. Kanjanaboos, C. T. O. Wong, J. J. McDowell, J. Xu, O. Voznyy, Z. Ning, A. J. Houtepen and E. H. Sargent, *Advanced Materials*, 2015, **27**, 53-58.
21. Y. Rong, Y. Ming, W. Ji, D. Li, A. Mei, Y. Hu and H. Han, *The Journal of Physical Chemistry Letters*, 2018, **9**, 2707-2713.
22. K. Cao, Z. Zuo, J. Cui, Y. Shen, T. Moehl, S. M. Zakeeruddin, M. Grätzel and M. Wang, *Nano Energy*, 2015, **17**, 171-179.
23. F. Mathies, H. Eggers, B. S. Richards, G. Hernandez-Sosa, U. Lemmer and U. W. Paetzold, *ACS Applied Energy Materials*, 2018, **1**, 1834-1839.
24. M. Saliba, J.-P. Correa-Baena, M. Grätzel, A. Hagfeldt and A. Abate, *Angewandte Chemie International Edition*, 2018, **57**, 2554-2569.
25. J. Yang, Y. Lin, W. Zheng, A. Liu, W. Cai, X. Yu, F. Zhang, Q. Liang, H. Wu, D. Qin and L. Hou, *ACS Applied Materials & Interfaces*, 2018, **10**, 22485-22494.
26. A. Kojima, K. Teshima, Y. Shirai and T. Miyasaka, *Journal of the American Chemical Society*, 2009, **131**, 6050-6051.
27. H.-S. Kim, C.-R. Lee, J.-H. Im, K.-B. Lee, T. Moehl, A. Marchioro, S.-J. Moon, R. Humphry-Baker, J.-H. Yum, J. E. Moser, M. Grätzel and N.-G. Park, *Scientific Reports*, 2012, **2**, 591.
28. M. M. Lee, J. Teuscher, T. Miyasaka, T. N. Murakami and H. J. Snaith, *Science*, 2012, **338**, 643-647.

29. M. Saliba, T. Matsui, J.-Y. Seo, K. Domanski, J.-P. Correa-Baena, M. K. Nazeeruddin, S. M. Zakeeruddin, W. Tress, A. Abate, A. Hagfeldt and M. Grätzel, *Energy & Environmental Science*, 2016, **9**, 1989-1997.
30. C. Huang, W. Fu, C.-Z. Li, Z. Zhang, W. Qiu, M. Shi, P. Heremans, A. K. Y. Jen and H. Chen, *Journal of the American Chemical Society*, 2016, **138**, 2528-2531.
31. Q. Wang and A. Abate, *Advanced Materials Interfaces*, **0**, 1800264.
32. L. K. Ono, Y. Qi and S. Liu, *Joule*, DOI: 10.1016/j.joule.2018.07.007.
33. M. Saliba, M. Stolterfoht, C. M. Wolff, D. Neher and A. Abate, *Joule*, 2018, **2**, 1019-1024.
34. M. O. Reese, S. A. Gevorgyan, M. Jørgensen, E. Bundgaard, S. R. Kurtz, D. S. Ginley, D. C. Olson, M. T. Lloyd, P. Morvillo, E. A. Katz, A. Elschner, O. Haillant, T. R. Currier, V. Shrotriya, M. Hermenau, M. Riede, K. R. Kirov, G. Trimmel, T. Rath, O. Inganäs, F. Zhang, M. Andersson, K. Tvingstedt, M. Lira-Cantu, D. Laird, C. McGuiness, S. Gowrisanker, M. Pannone, M. Xiao, J. Hauch, R. Steim, D. M. DeLongchamp, R. Rösch, H. Hoppe, N. Espinosa, A. Urbina, G. Yaman-Uzunoglu, J.-B. Bonekamp, A. J. J. M. van Breemen, C. Girotto, E. Voroshazi and F. C. Krebs, *Solar Energy Materials and Solar Cells*, 2011, **95**, 1253-1267.
35. J. A. Christians, P. Schulz, J. S. Tinkham, T. H. Schloemer, S. P. Harvey, B. J. Tremolet de Villers, A. Sellinger, J. J. Berry and J. M. Luther, *Nature Energy*, 2018, **3**, 68-74.
36. A. Tiihonen, K. Miettunen, J. Halme, S. Lepikko, A. Poskela and P. D. Lund, *Energy & Environmental Science*, 2018, **11**, 730-738.
37. M. Saliba, J.-P. Correa-Baena, C. M. Wolff, M. Stolterfoht, N. Phung, S. Albrecht, D. Neher and AbateAntonio, *Chemistry of Materials*, 2017.
38. M. Saliba, J.-P. Correa-Baena, C. M. Wolff, M. Stolterfoht, N. Phung, S. Albrecht, D. Neher and A. Abate, *Chemistry of Materials*, 2017.
39. S. Sun, T. Buonassisi and J.-P. Correa-Baena, *Advanced Materials Interfaces*, **0**, 1800408.
40. Q. Dong, Y. Shi, C. Zhang, Y. Wu and L. Wang, *Nano Energy*, 2017, **40**, 336-344.
41. K. Wojciechowski, M. Saliba, T. Leijtens, A. Abate and H. J. Snaith, *Energy & Environmental Science*, 2014, **7**, 1142-1147.
42. D. Yang, R. Yang, J. Zhang, Z. Yang, S. Liu and C. Li, *Energy & Environmental Science*, 2015, **8**, 3208-3214.
43. H. J. Snaith, A. Abate, J. M. Ball, G. E. Eperon, T. Leijtens, N. K. Noel, S. D. Stranks, J. T.-W. Wang, K. Wojciechowski and W. Zhang, *The journal of physical chemistry letters*, 2014, **5**, 1511-1515.
44. F. Giordano, A. Abate, J. P. Correa Baena, M. Saliba, T. Matsui, S. H. Im, S. M. Zakeeruddin, M. K. Nazeeruddin, A. Hagfeldt and M. Graetzel, *Nature Communications*, 2016, **7**, 10379.
45. T. Leijtens, G. E. Eperon, S. Pathak, A. Abate, M. M. Lee and H. J. Snaith, *Nature Communications*, 2013, **4**, 2885.
46. H. J. Jung, D. Kim, S. Kim, J. Park, V. P. Dravid and B. Shin, *Advanced Materials*, **0**, 1802769.
47. J. Cao, X. Lv, P. Zhang, T. T. Chuong, B. Wu, X. Feng, C. Shan, J. Liu and Y. Tang, *Adv Mater*, 2018, **30**, e1800568.
48. Q. Wali, A. Fakharuddin and R. Jose, *Journal of Power Sources*, 2015, **293**, 1039-1052.
49. J. P. Correa Baena, L. Steier, W. Tress, M. Saliba, S. Neutzner, T. Matsui, F. Giordano, T. J. Jacobsson, A. R. Srimath Kandada, S. M. Zakeeruddin, A. Petrozza, A. Abate, M. K. Nazeeruddin, M. Gratzel and A. Hagfeldt, *Energy & Environmental Science*, 2015, **8**, 2928-2934.
50. B. Roose, C. M. Johansen, K. Dupraz, T. Jaouen, P. Aebi, U. Steiner and A. Abate, *Journal of Materials Chemistry A*, 2018, **6**, 1850-1857.
51. W. Nie, J.-C. Blancon, A. J. Neukirch, K. Appavoo, H. Tsai, M. Chhowalla, M. A. Alam, M. Y. Sfeir, C. Katan, J. Even, S. Tretiak, J. J. Crochet, G. Gupta and A. D. Mohite, *Nature Communications*, 2016, **7**, 11574.
52. K. H. Il, K. Myeong-Jong, C. Kyoungwon, L. Chaesung, K. Yun-Hi, K. Soon-Ki and P. Taiho, *Advanced Energy Materials*, 2018, **8**, 1702872.
53. G.-H. Kim, H. Jang, Y. J. Yoon, J. Jeong, S. Y. Park, B. Walker, I.-Y. Jeon, Y. Jo, H. Yoon, M. Kim, J.-B. Baek, D. S. Kim and J. Y. Kim, *Nano Letters*, 2017, **17**, 6385-6390.

54. M. Stolterfoht, C. M. Wolff, Y. Amir, A. Paulke, L. Perdigon-Toro, P. Caprioglio and D. Neher, *Energy & Environmental Science*, 2017, **10**, 1530-1539.
55. Y. Wang, Y. Liang, Y. Zhang, W. Yang, L. Sun and D. Xu, *Advanced Functional Materials*, 2018, 1801237.
56. D.-Y. Son, J.-W. Lee, Y. J. Choi, I.-H. Jang, S. Lee, P. J. Yoo, H. Shin, N. Ahn, M. Choi and D. Kim, *Nature Energy*, 2016, **1**, 16081.
57. Y. Han, S. Meyer, Y. Dkhissi, K. Weber, J. M. Pringle, U. Bach, L. Spiccia and Y.-B. Cheng, *Journal of Materials Chemistry A*, 2015, **3**, 8139-8147.
58. B. Conings, J. Drijkoningen, N. Gauquelin, A. Babayigit, J. D'Haen, L. D'Olieslaeger, A. Ethirajan, J. Verbeeck, J. Manca and E. Mosconi, *Advanced Energy Materials*, 2015, **5**.
59. N. Aristidou, I. Sanchez-Molina, T. Chotchuangchutchaval, M. Brown, L. Martinez, T. Rath and S. A. Haque, *Angewandte Chemie*, 2015, **127**, 8326-8330.
60. M. Jung, T. J. Shin, J. Seo, G. Kim and S. I. Seok, *Energy & Environmental Science*, 2018.
61. N. Ahn, K. Kwak, M. S. Jang, H. Yoon, B. Y. Lee, J.-K. Lee, P. V. Pikhitsa, J. Byun and M. Choi, *Nature Communications*, 2016, **7**, 13422.
62. J. H. Noh, S. H. Im, J. H. Heo, T. N. Mandal and S. I. Seok, *Nano letters*, 2013, **13**, 1764-1769.
63. K. L. Svane, A. C. Forse, C. P. Grey, G. Kieslich, A. K. Cheetham, A. Walsh and K. T. Butler, *The Journal of Physical Chemistry Letters*, 2017, **8**, 6154-6159.
64. J. A. Christians, P. A. Miranda Herrera and P. V. Kamat, *Journal of the American Chemical Society*, 2015, **137**, 1530-1538.
65. A. Merdasa, M. Bag, Y. Tian, E. Källman, A. Dobrovolsky and I. G. Scheblykin, *The Journal of Physical Chemistry C*, 2016, **120**, 10711-10719.
66. X. Zheng, C. Wu, S. K. Jha, Z. Li, K. Zhu and S. Priya, *ACS Energy Letters*, 2016, **1**, 1014-1020.
67. D. M. Jang, K. Park, D. H. Kim, J. Park, F. Shojaei, H. S. Kang, J.-P. Ahn, J. W. Lee and J. K. Song, *Nano letters*, 2015, **15**, 5191-5199.
68. E. T. Hoke, D. J. Slotcavage, E. R. Dohner, A. R. Bowring, H. I. Karunadasa and M. D. McGehee, *Chemical Science*, 2015, **6**, 613-617.
69. T. Umebayashi, K. Asai, T. Kondo and A. Nakao, *Physical Review B*, 2003, **67**, 155405.
70. D. Meggiolaro, S. G. Motti, E. Mosconi, A. J. Barker, J. Ball, C. Andrea Riccardo Perini, F. Deschler, A. Petrozza and F. De Angelis, *Energy & Environmental Science*, 2018, **11**, 702-713.
71. E. Mosconi, D. Meggiolaro, H. J. Snaith, S. D. Stranks and F. De Angelis, *Energy & Environmental Science*, 2016, **9**, 3180-3187.
72. P. Delugas, A. Filippetti and A. Mattoni, *Physical Review B*, 2015, **92**, 045301.
73. A. Sadhanala, S. Ahmad, B. Zhao, N. Giesbrecht, P. M. Pearce, F. Deschler, R. L. Hoye, K. C. Gödel, T. Bein and P. Docampo, *Nano letters*, 2015, **15**, 6095-6101.
74. F. Brivio, C. Caetano and A. Walsh, *The journal of physical chemistry letters*, 2016, **7**, 1083-1087.
75. C. G. Bischak, C. L. Hetherington, H. Wu, S. Aloni, D. F. Ogletree, D. T. Limmer and N. S. Ginsberg, *Nano letters*, 2017, **17**, 1028-1033.
76. C. G. Bischak, A. B. Wong, E. Lin, D. T. Limmer, P. Yang and N. S. Ginsberg, *The journal of physical chemistry letters*, 2018, **9**, 3998-4005.
77. A. J. Barker, A. Sadhanala, F. Deschler, M. Gandini, S. P. Senanayak, P. M. Pearce, E. Mosconi, A. J. Pearson, Y. Wu, A. R. Srimath Kandada, T. Leijtens, F. De Angelis, S. E. Dutton, A. Petrozza and R. H. Friend, *ACS Energy Letters*, 2017, **2**, 1416-1424.
78. D. J. Slotcavage, H. I. Karunadasa and M. D. McGehee, *ACS Energy Letters*, 2016, **1**, 1199-1205.
79. F. Zhu, L. Men, Y. Guo, Q. Zhu, U. Bhattacharjee, P. M. Goodwin, J. W. Petrich, E. A. Smith and J. Vela, *ACS nano*, 2015, **9**, 2948-2959.
80. S. J. Yoon, M. Kuno and P. V. Kamat, *Acs Energy Letters*, 2017, **2**, 1507-1514.
81. W. Rehman, D. P. McMeekin, J. B. Patel, R. L. Milot, M. B. Johnston, H. J. Snaith and L. M. Herz, *Energy & Environmental Science*, 2017, **10**, 361-369.
82. X. Tang, M. van den Berg, E. Gu, A. Horneber, G. J. Matt, A. Osvet, A. J. Meixner, D. Zhang and C. J. Brabec, *Nano letters*, 2018, **18**, 2172-2178.
83. C. C. Stoumpos, D. H. Cao, D. J. Clark, J. Young, J. M. Rondinelli, J. I. Jang, J. T. Hupp and M. G. Kanatzidis, *Chemistry of Materials*, 2016, **28**, 2852-2867.

84. J. Xing, Q. Wang, Q. Dong, Y. Yuan, Y. Fang and J. Huang, *Physical Chemistry Chemical Physics*, 2016, **18**, 30484-30490.
85. G. E. Eperon, S. D. Stranks, C. Menelaou, M. B. Johnston, L. M. Herz and H. J. Snaith, *Energy & Environmental Science*, 2014, **7**, 982-988.
86. M. Saliba, T. Matsui, K. Domanski, J.-Y. Seo, A. Ummadisingu, S. M. Zakeeruddin, J.-P. Correa-Baena, W. R. Tress, A. Abate, A. Hagfeldt and M. Grätzel, *Science*, 2016, **354**, 206-209.
87. P. Luo, W. Xia, S. Zhou, L. Sun, J. Cheng, C. Xu and Y. Lu, *The Journal of Physical Chemistry Letters*, 2016, **7**, 3603-3608.
88. F. Haque, M. Wright, M. A. Mahmud, H. Yi, D. Wang, L. Duan, C. Xu, M. B. Upama and A. Uddin, *ACS Omega*, 2018, **3**, 11937-11944.
89. D. Y. Heo, S. M. Han, N. S. Woo, Y. J. Kim, T.-Y. Kim, Z. Luo and S. Y. Kim, *The Journal of Physical Chemistry C*, 2018, **122**, 15903-15910.
90. W. Shockley and H. J. Queisser, *Journal of applied physics*, 1961, **32**, 510-519.
91. C. C. Stoumpos, C. D. Malliakas and M. G. Kanatzidis, *Inorganic chemistry*, 2013, **52**, 9019-9038.
92. W. S. Yang, B.-W. Park, E. H. Jung, N. J. Jeon, Y. C. Kim, D. U. Lee, S. S. Shin, J. Seo, E. K. Kim, J. H. Noh and S. I. Seok, *Science*, 2017, **356**, 1376-1379.
93. O. A. Syzgantseva, M. Saliba, M. Grätzel and U. Rothlisberger, *The journal of physical chemistry letters*, 2017, **8**, 1191-1196.
94. C. Yi, J. Luo, S. Meloni, A. Boziki, N. Ashari-Astani, C. Grätzel, S. M. Zakeeruddin, U. Röthlisberger and M. Grätzel, *Energy & Environmental Science*, 2016, **9**, 656-662.
95. D. P. McMeekin, G. Sadoughi, W. Rehman, G. E. Eperon, M. Saliba, M. T. Hörantner, A. Haghighirad, N. Sakai, L. Korte, B. Rech, M. B. Johnston, L. M. Herz and H. J. Snaith, *Science*, 2016, **351**, 151-155.
96. M. Abdi-Jalebi, Z. Andaji-Garmaroudi, S. Cacovich, C. Stavrakas, B. Philippe, J. M. Richter, M. Alsari, E. P. Booker, E. M. Hutter and A. J. Pearson, *Nature*, 2018, **555**, 497.
97. T. Duong, Y. Wu, H. Shen, J. Peng, X. Fu, D. Jacobs, E. C. Wang, T. C. Kho, K. C. Fong and M. Stocks, *Advanced Energy materials*, 2017, **7**.
98. K. Y. Chiu, S. H. Chang, W.-C. Huang, H.-M. Cheng, H. Shaw, S.-C. Yeh, C.-T. Chen, Y. O. Su, S.-H. Chen and C.-G. Wu, *Nanotechnology*, 2018, **29**, 305701.
99. D.-Y. Son, S.-G. Kim, J.-Y. Seo, S.-H. Lee, H. Shin, D. Lee and N.-G. Park, *Journal of the American Chemical Society*, 2018.
100. J. Cao, S. X. Tao, P. A. Bobbert, C. P. Wong and N. Zhao, *Advanced Materials*, 2018, 1707350.
101. B. Philippe, M. Saliba, J.-P. Correa-Baena, U. B. Cappel, S.-H. Turren-Cruz, M. Grätzel, A. Hagfeldt and H. k. Rensmo, *Chemistry of Materials*, 2017, **29**, 3589-3596.
102. T. J. Jacobsson, S. Svanström, V. Andrei, J. P. Rivett, N. Kornienko, B. Philippe, U. B. Cappel, H. k. Rensmo, F. Deschler and G. Boschloo, *The Journal of Physical Chemistry C*, 2018.
103. D. J. Kubicki, D. Prochowicz, A. Hofstetter, S. M. Zakeeruddin, M. Grätzel and L. Emsley, *Journal of the American Chemical Society*, 2017, **139**, 14173-14180.
104. A. Albadri, P. Yadav, M. Alotaibi, N. Arora, A. Alyamani, H. Albrithen, M. I. Dar, S. M. Zakeeruddin and M. Grätzel, *The Journal of Physical Chemistry C*, 2017, **121**, 24903-24908.
105. D. Yao, C. Zhang, N. D. Pham, Y. Zhang, V. T. Tiong, A. Du, Q. Shen, G. J. Wilson and H. Wang, *The journal of physical chemistry letters*, 2018, **9**, 2113-2120.
106. B. Li, Y. Zhang, L. Fu, T. Yu, S. Zhou, L. Zhang and L. Yin, *Nature communications*, 2018, **9**, 1076.
107. Q. Wang, X. Zheng, Y. Deng, J. Zhao, Z. Chen and J. Huang, *Joule*, 2017, **1**, 371-382.
108. P. Wang, X. Zhang, Y. Zhou, Q. Jiang, Q. Ye, Z. Chu, X. Li, X. Yang, Z. Yin and J. You, *Nature communications*, 2018, **9**, 2225.
109. M. Kulbak, S. Gupta, N. Kedem, I. Levine, T. Bendikov, G. Hodes and D. Cahen, *The journal of physical chemistry letters*, 2015, **7**, 167-172.
110. G. E. Eperon, G. M. Paterno, R. J. Sutton, A. Zampetti, A. A. Haghighirad, F. Cacialli and H. J. Snaith, *Journal of Materials Chemistry A*, 2015, **3**, 19688-19695.
111. R. J. Sutton, G. E. Eperon, L. Miranda, E. S. Parrott, B. A. Kamino, J. B. Patel, M. T. Hörantner, M. B. Johnston, A. A. Haghighirad and D. T. Moore, *Advanced Energy Materials*, 2016, **6**.

112. A. Swarnkar, A. R. Marshall, E. M. Sanehira, B. D. Chernomordik, D. T. Moore, J. A. Christians, T. Chakrabarti and J. M. Luther, *Science*, 2016, **354**, 92-95.
113. T. Zhang, M. I. Dar, G. Li, F. Xu, N. Guo, M. Grätzel and Y. Zhao, *Science advances*, 2017, **3**, e1700841.
114. R. J. Sutton, M. R. Filip, A. A. Haghighirad, N. Sakai, B. Wenger, F. Giustino and H. J. Snaith, *ACS Energy Letters*, 2018, **3**, 1787-1794.
115. C. Y. Chen, H. Y. Lin, K. M. Chiang, W. L. Tsai, Y. C. Huang, C. S. Tsao and H. W. Lin, *Advanced materials*, 2017, **29**, 1605290.
116. C. Liu, W. Li, C. Zhang, Y. Ma, J. Fan and Y. Mai, *Journal of the American Chemical Society*, 2018, **140**, 3825-3828.
117. J. K. Nam, M. S. Jung, S. U. Chai, Y. J. Choi, D. Kim and J. H. Park, *The Journal of Physical Chemistry Letters*, 2017, **8**, 2936-2940.
118. S. Sanchez, N. Christoph, B. Grobety, N. Phung, U. Steiner, M. Saliba and A. Abate, *Advanced Energy Materials*, 2018.
119. R. E. Beal, D. J. Slotcavage, T. Leijtens, A. R. Bowring, R. A. Belisle, W. H. Nguyen, G. F. Burkhard, E. T. Hoke and M. D. McGehee, *The journal of physical chemistry letters*, 2016, **7**, 746-751.
120. Q. A. Akkerman, V. D'Innocenzo, S. Accornero, A. Scarpellini, A. Petrozza, M. Prato and L. Manna, *Journal of the American Chemical Society*, 2015, **137**, 10276-10281.
121. K. Domanski, B. Roose, T. Matsui, M. Saliba, S.-H. Turren-Cruz, J.-P. Correa-Baena, C. R. Carmona, G. Richardson, J. M. Foster, F. De Angelis, J. M. Ball, A. Petrozza, N. Mine, M. K. Nazeeruddin, W. Tress, M. Grätzel, U. Steiner, A. Hagfeldt and A. Abate, *Energy & Environmental Science*, 2017, **10**, 604-613.
122. Y. Hu, F. Bai, X. Liu, Q. Ji, X. Miao, T. Qiu and S. Zhang, *ACS Energy Letters*, 2017, **2**, 2219-2227.
123. H. Tsai, W. Nie, J.-C. Blancon, C. C. Stoumpos, R. Asadpour, B. Harutyunyan, A. J. Neukirch, R. Verduzco, J. J. Crochet, S. Tretiak, L. Pedesseau, J. Even, M. A. Alam, G. Gupta, J. Lou, P. M. Ajayan, M. J. Bedzyk, M. G. Kanatzidis and A. D. Mohite, *Nature*, 2016, **536**, 312.
124. Z. Wang, Q. Lin, F. P. Chmiel, N. Sakai, L. M. Herz and H. J. Snaith, *Nature Energy*, 2017, **2**, 17135.
125. D. H. Cao, C. C. Stoumpos, O. K. Farha, J. T. Hupp and M. G. Kanatzidis, *Journal of the American Chemical Society*, 2015, **137**, 7843-7850.
126. S. I. C., H. E. T., S. I. Diego, M. M. D. and K. H. I., *Angewandte Chemie*, 2014, **126**, 11414-11417.
127. X. Zhang, X. Ren, B. Liu, R. Munir, X. Zhu, D. Yang, J. Li, Y. Liu, D.-M. Smilgies, R. Li, Z. Yang, T. Niu, X. Wang, A. Amassian, K. Zhao and S. Liu, *Energy & Environmental Science*, 2017, **10**, 2095-2102.
128. Z. Xinqian, W. Gang, F. Weifei, Q. Minchao, Y. Weitao, Y. Jielin, Z. Zhongqiang, L. Xinhui and C. Hongzheng, *Advanced Energy Materials*, 2018, **8**, 1702498.
129. Q. Wang, C. Jiang, P. Zhang and T. W. Hamann, *The Journal of Physical Chemistry C*, 2018, DOI: 10.1021/acs.jpcc.8b01592.
130. G. Giorgi, K. Yamashita and M. Palummo, *The Journal of Physical Chemistry Letters*, 2018, DOI: 10.1021/acs.jpclett.8b02653, 5891-5896.
131. J.-P. Correa-Baena, A. Abate, M. Saliba, W. Tress, T. Jesper Jacobsson, M. Gratzel and A. Hagfeldt, *Energy & Environmental Science*, 2017, **10**, 710-727.
132. M. Deepa, M. Salado, L. Calio, S. Kazim, S. M. Shivaprasad and S. Ahmad, *Physical Chemistry Chemical Physics*, 2017, **19**, 4069-4077.
133. J. Endres, D. A. Egger, M. Kulbak, R. A. Kerner, L. Zhao, S. H. Silver, G. Hodes, B. P. Rand, D. Cahen, L. Kronik and A. Kahn, *The Journal of Physical Chemistry Letters*, 2016, **7**, 2722-2729.
134. S. Ryu, J. H. Noh, N. J. Jeon, Y. Chan Kim, W. S. Yang, J. Seo and S. I. Seok, *Energy & Environmental Science*, 2014, **7**, 2614-2618.
135. P. Schulz, *ACS Energy Letters*, 2018, **3**, 1287-1293.
136. Y. Weibo, Y. Senyun, L. Yunlong, S. Weihai, R. Haixia, L. Zhiwei, B. Zuqiang and H. Chunhui, *Advanced Energy Materials*, 2016, **6**, 1600474.
137. Z. H. Bakr, Q. Wali, A. Fakharuddin, L. Schmidt-Mende, T. M. Brown and R. Jose, *Nano Energy*, 2017, **34**, 271-305.

138. C. Wei, Z. Yecheng, W. Linjing, W. Yinghui, T. Bao, Y. Binbin, L. Fangzhou, T. Ho-Won, W. Gan, D. A. B., H. Li and H. Zhubing, *Advanced Materials*, 2018, **30**, 1800515.
139. L. Ziye, C. Jingjing, L. Zhenhua, Z. Long, Y. Zhou, C. Dazheng, Z. Chunfu, L. Shengzhong and H. Yue, *Advanced Energy Materials*, 2018, **8**, 1703432.
140. N. Wanyi, T. Hsinhan, B. Jean-Christophe, L. Fangze, S. C. C., T. Boubacar, K. Mikael, D. Olivier, K. Claudine, T. Sergei, C. Jared, A. P. M., K. MercouriG., E. Jacky and M. A. D., *Advanced Materials*, 2018, **30**, 1703879.
141. G. M. T., C. Lily, H. M. G., T. Wing-Man and L. Zheng-Hong, *Advanced Functional Materials*, 2012, **22**, 4557-4568.
142. L. Ming-Wei, W. Kuo-Chin, W. Jeng-Han, L. Ming-Hsien, L. Yu-Ling, O. Takuji, K. Nobuhiro, C. Peter, W. Der-Hsin, G. Tzung-Fang and H. Yao-Jane, *Advanced Materials Interfaces*, 2016, **3**, 1600135.
143. V. Roiati, E. Mosconi, A. Listorti, S. Colella, G. Gigli and F. De Angelis, *Nano Letters*, 2014, **14**, 2168-2174.
144. C. Jordi, G. Antonio, R. Sara, A. Osbel, Z. Issac, M.-M. Elena, B. Juan and G.-B. Germà, *Advanced Energy Materials*, 2016, **6**, 1502246.
145. R. A. Kerner and B. P. Rand, *The Journal of Physical Chemistry Letters*, 2017, **8**, 2298-2303.
146. S. A. L. Weber, I. M. Hermes, S.-H. Turren-Cruz, C. Gort, V. W. Bergmann, L. Gilson, A. Hagfeldt, M. Graetzel, W. Tress and R. Berger, *Energy & Environmental Science*, 2018, DOI: 10.1039/C8EE01447G.
147. P. Schulz, J. O. Tiepelt, J. A. Christians, I. Levine, E. Edri, E. M. Sanehira, G. Hodes, D. Cahen and A. Kahn, *ACS Applied Materials & Interfaces*, 2016, **8**, 31491-31499.
148. M. Acik, I. K. Park, R. E. Koritala, G. Lee and R. A. Rosenberg, *Journal of Materials Chemistry A*, 2018, **6**, 1423-1442.
149. W. Chen, Y. Wu, Y. Yue, J. Liu, W. Zhang, X. Yang, H. Chen, E. Bi, I. Ashraful, M. Grätzel and L. Han, *Science*, 2015, **350**, 944-948.
150. H. Tsai, R. Asadpour, J.-C. Blancon, C. C. Stoumpos, O. Durand, J. W. Strzalka, B. Chen, R. Verduzco, P. M. Ajayan, S. Tretiak, J. Even, M. A. Alam, M. G. Kanatzidis, W. Nie and A. D. Mohite, *Science*, 2018, **360**, 67-70.
151. S. Shao, M. Abdu-Aguye, L. Qiu, L.-H. Lai, J. Liu, S. Adjokatse, F. Jahani, M. E. Kamminga, G. H. ten Brink, T. T. M. Palstra, B. J. Kooi, J. C. Hummelen and M. Antonietta Loi, *Energy & Environmental Science*, 2016, **9**, 2444-2452.
152. T. Zhang, S. H. Cheung, X. Meng, L. Zhu, Y. Bai, C. H. Y. Ho, S. Xiao, Q. Xue, S. K. So and S. Yang, *The Journal of Physical Chemistry Letters*, 2017, **8**, 5069-5076.
153. Z. Hua, W. Huan, Z. Hongmei, C. Chu-Chen, C. Wei, Y. Shihe and J. A. K.-Y., *Advanced Energy Materials*, 2018, **8**, 1702762.
154. M. B. Islam, M. Yanagida, Y. Shirai, Y. Nabetani and K. Miyano, *ACS Omega*, 2017, **2**, 2291-2299.
155. S. Schuller, P. Schilinsky, J. Hauch and C. J. Brabec, *Applied Physics A*, 2004, **79**, 37-40.
156. C.-H. Chiang, C.-C. Chen, M. K. Nazeeruddin and C.-G. Wu, *Journal of Materials Chemistry A*, 2018, DOI: 10.1039/C8TA05264F.
157. O. Dan, X. Junyan, Y. Fei, H. Zhanfeng, Z. Hong, Z. Lu, C. Jiaqi and C. W. C. H., *Advanced Energy Materials*, 2018, **8**, 1702722.
158. N. Arora, M. I. Dar, A. Hinderhofer, N. Pellet, F. Schreiber, S. M. Zakeeruddin and M. Grätzel, *Science*, 2017, DOI: 10.1126/science.aam5655.
159. Z. Liu, A. Zhu, F. Cai, L. Tao, Y. Zhou, Z. Zhao, Q. Chen, Y.-B. Cheng and H. Zhou, *Journal of Materials Chemistry A*, 2017, **5**, 6597-6605.
160. B. A. R., B. Luca, O. R. B. C. and M. M. D., *Advanced Energy Materials*, 2018, **8**, 1702365.
161. A. Rajagopal, S. T. Williams, C.-C. Chueh and A. K. Y. Jen, *The Journal of Physical Chemistry Letters*, 2016, **7**, 995-1003.
162. T. Malinauskas, D. Tomkute-Luksiene, R. Sens, M. Daskeviciene, R. Send, H. Wonneberger, V. Jankauskas, I. Bruder and V. Getautis, *ACS Applied Materials & Interfaces*, 2015, **7**, 11107-11116.

163. U. Bach, D. Lupo, P. Comte, J. E. Moser, F. Weissörtel, J. Salbeck, H. Spreitzer and M. Grätzel, *Nature*, 1998, **395**, 583.
164. Y. Hu, E. M. Hutter, P. Rieder, I. Grill, J. Hanisch, M. F. Aygüler, A. G. Hufnagel, M. Handloser, T. Bein and A. Hartschuh, *Advanced Energy Materials*, 2018, 1703057.
165. , DOI: http://www.sigmaaldrich.com/catalog/product/aldrich/702471?lang=fi&region=FI.
166. A. T. Murray, J. M. Frost, C. H. Hendon, C. D. Molloy, D. R. Carbery and A. Walsh, *Chemical Communications*, 2015, **51**, 8935-8938.
167. *KTH Chemical Science and Engineering*, 2015.
168. E. J. Juarez-Perez, M. R. Leyden, S. Wang, L. K. Ono, Z. Hawash and Y. Qi, *Chemistry of Materials*, 2016, **28**, 5702-5709.
169. M. Ulfa, T. Zhu, F. Goubard and T. Pauporte, *Journal of Materials Chemistry A*, 2018, DOI: 10.1039/C8TA03875A.
170. S. Guarnera, A. Abate, W. Zhang, J. M. Foster, G. Richardson, A. Petrozza and H. J. Snaith, *The Journal of Physical Chemistry Letters*, 2015, **6**, 432-437.
171. P. Sanghyun, Q. Peng, L. Yonghui, C. K. Taek, G. Peng, G. Giulia, O. Emad, G. Paul, R. Kasparas, A.-M. S. A., L. Christian, K. Jaejung and N. M. Khaja, *Advanced Materials*, 2017, **29**, 1606555.
172. P. H. Duc, D. T. Trang, K. Jinhyun, C. Cecile, M. Sergei, F. Krishna, T. W. Chung, D. J. R., J. S. M. and S. Prashant, *Advanced Energy Materials*, 2018, **8**, 1703007.
173. X. Bo, Z. Zonglong, Z. Jinbao, L. Hongbin, C. Chu-Chen, L. Xiaosong and J. A. K.-Y., *Advanced Energy Materials*, 2017, **7**, 1700683.
174. J. Liu, Y. Wu, C. Qin, X. Yang, T. Yasuda, A. Islam, K. Zhang, W. Peng, W. Chen and L. Han, *Energy & Environmental Science*, 2014, **7**, 2963-2967.
175. J. H. Heo, S. Park, S. H. Im and H. J. Son, *ACS Applied Materials & Interfaces*, 2017, **9**, 39511-39518.
176. G.-W. Kim, G. Kang, J. Kim, G.-Y. Lee, H. I. Kim, L. Pyeon, J. Lee and T. Park, *Energy & Environmental Science*, 2016, **9**, 2326-2333.
177. J. Lee, M. Malekshahi Byranvand, G. Kang, S. Y. Son, S. Song, G.-W. Kim and T. Park, *Journal of the American Chemical Society*, 2017, **139**, 12175-12181.
178. K. Guan-Woo, L. Junwoo, K. Gyeongho, K. Taewan and P. Taiho, *Advanced Energy Materials*, 2018, **8**, 1701935.
179. Z. Weiqi, W. Zhenhai and G. Peng, *Advanced Energy Materials*, 2018, **8**, 1702512.
180. P. Vivo, J. Salunke and A. Priimagi, *Materials*, 2017, **10**, 1087.
181. E. Raza, F. Aziz and Z. Ahmad, *RSC Advances*, 2018, **8**, 20952-20967.
182. H. Zheng, G. Liu, L. Zhu, J. Ye, X. Zhang, A. Alsaedi, T. Hayat, X. Pan and S. Dai, *ACS Applied Materials & Interfaces*, 2017, **9**, 41006-41013.
183. K. Domanski, B. Roose, T. Matsui, M. Saliba, S.-H. Turren-Cruz, J.-P. Correa-Baena, C. R. Carmona, G. Richardson, J. M. Foster, F. De Angelis, J. M. Ball, A. Petrozza, N. Mine, M. K. Nazeeruddin, W. Tress, M. Gratzel, U. Steiner, A. Hagfeldt and A. Abate, *Energy & Environmental Science*, 2017, **10**, 604-613.
184. W. H. Nguyen, C. D. Bailie, E. L. Unger and M. D. McGehee, *Journal of the American Chemical Society*, 2014, **136**, 10996-11001.
185. T. Leijtens, T. Giovenzana, S. N. Habisreutinger, J. S. Tinkham, N. K. Noel, B. A. Kamino, G. Sadoughi, A. Sellinger and H. J. Snaith, *ACS Applied Materials & Interfaces*, 2016, **8**, 5981-5989.
186. X. Zhao, H.-S. Kim, J.-Y. Seo and N.-G. Park, *ACS Applied Materials & Interfaces*, 2017, **9**, 7148-7153.
187. I. Mesquita, L. Andrade and A. Mendes, *Renewable and Sustainable Energy Reviews*, 2018, **82**, 2471-2489.
188. K. Domanski, J.-P. Correa-Baena, N. Mine, M. K. Nazeeruddin, A. Abate, M. Saliba, W. Tress, A. Hagfeldt and M. Grätzel, *ACS Nano*, 2016, **10**, 6306-6314.
189. M. Anaya, J. P. Correa-Baena, G. Lozano, M. Saliba, P. Anguita, B. Roose, A. Abate, U. Steiner, M. Grätzel, M. E. Calvo, A. Hagfeldt and H. Míguez, *J Mater Chem A Mater Energy Sustain*, 2016, **4**, 11214-11221.

190. M. Taisuke, P. Ieva, M. Tadas, D. Konrad, D. Maryte, S. Matas, G. Paul, T. Wolfgang, C.-B. Juan-Pablo, A. Antonio, H. Anders, G. Michael, N. M. Khaja, G. Vytautas and S. Michael, *ChemSusChem*, 2016, **9**, 2567-2571.
191. F. Behrouznejad, S. Shahbazi, N. Taghavinia, H.-P. Wu and E. Wei-Guang Diau, *Journal of Materials Chemistry A*, 2016, **4**, 13488-13498.
192. P. Gratia, A. Magomedov, T. Malinauskas, M. Daskeviciene, A. Abate, S. Ahmad, M. Grätzel, V. Getautis and M. K. Nazeeruddin, *Angewandte Chemie International Edition*, 2015, **54**, 11409-11413.
193. H. J. Snaith, A. J. Moule, C. Klein, K. Meerholz, R. H. Friend and M. Grätzel, *Nano Letters*, 2007, **7**, 3372-3376.
194. H. Back, G. Kim, J. Kim, J. Kong, T. K. Kim, H. Kang, H. Kim, J. Lee, S. Lee and K. Lee, *Energy & Environmental Science*, 2016, **9**, 1258-1263.
195. N. Shlenskaya, N. A. Belich, M. Gratzel, E. A. Goodilin and A. B. Tarasov, *Journal of Materials Chemistry A*, 2018, **6**, 1780-1786.
196. S. Cacovich, L. Cina, F. Matteocci, G. Divitini, P. A. Midgley, A. Di Carlo and C. Ducati, *Nanoscale*, 2017, **9**, 4700-4706.
197. A. Kerttu, D. Konrad, C.-B. Juan-Pablo, S. Kári, S. Michael, A. Antonio, G. Michael, K. Esko, J. E. M. J., T. Wolfgang, H. Anders and B. Gerrit, *Advanced Materials*, 2017, **29**, 1606398.
198. I. Jeon, S. Seo, Y. Sato, C. Delacou, A. Anisimov, K. Suenaga, E. I. Kauppinen, S. Maruyama and Y. Matsuo, *The Journal of Physical Chemistry C*, 2017, **121**, 25743-25749.
199. P. Jiang, Y. Xiong, M. Xu, A. Mei, Y. Sheng, L. Hong, T. W. Jones, G. J. Wilson, S. Xiong, D. Li, Y. Hu, Y. Rong and H. Han, *The Journal of Physical Chemistry C*, 2018, **122**, 16481-16487.
200. C. Tian, A. Mei, S. Zhang, H. Tian, S. Liu, F. Qin, Y. Xiong, Y. Rong, Y. Hu, Y. Zhou, S. Xie and H. Han, *Nano Energy*, 2018, DOI: https://doi.org/10.1016/j.nanoen.2018.08.050.
201. A. Swarnkar, W. J. Mir and A. Nag, *ACS Energy Letters*, 2018, **3**, 286-289.
202. W. Zhang, W. Yang, P. Zhong, S. Mei, G. Zhang, G. Chen, G. He and R. Guo, *Opt. Mater. Express*, 2017, **7**, 3065-3076.
203. W. Xiang, Z. Wang, D. J. Kubicki, W. Tress, J. Luo, D. Prochowicz, S. Akin, L. Emsley, J. Zhou, G. Dietler, M. Grätzel and A. Hagfeldt, *Joule*, DOI: 10.1016/j.joule.2018.10.008.
204. A. K. Jena, A. Kulkarni, Y. Sanehira, M. Ikegami and T. Miyasaka, *Chemistry of Materials*, 2018, **30**, 6668-6674.
205. Y. Wang, T. Zhang, M. Kan and Y. Zhao, *Journal of the American Chemical Society*, 2018, **140**, 12345-12348.
206. W. Xiang, Z. Wang, D. J. Kubicki, W. Tress, J. Luo, D. Prochowicz, S. Akin, L. Emsley, J. Zhou, G. Dietler, M. Grätzel and A. Hagfeldt, *Joule*, 2018, DOI: https://doi.org/10.1016/j.joule.2018.10.008.